APPENDIX A

JOINT COMMITTEE ON POWDER DIFFRACTION STANDARDS

1) Zn, JCPDS file number 04-0831

Crystal system	:	Hexagonal
Space group	:	P63/mmc
Space group number	:	194
a	:	2.6650
b	:	2.6650
c	:	4.9470
Alpha	:	90.0000
Beta	:	90.0000
Gamma	:	120.0000
Calculated density (g/cm^3)	:	7.13
Measured density (g/cm^3)	:	7.05
Volume of cell (10^6 pm^3)	:	30.43
Z	:	2.00

Peak list

No.	h	k	l	d [A]	2Theta[deg]	I [%]
1	0	0	2	2.47300	36.297	53.0
2	1	0	0	2.30800	38.993	40.0
3	1	0	1	2.09100	43.233	100.0
4	1	0	2	1.68700	54.337	28.0
5	1	0	3	1.34200	70.058	25.0
6	1	1	0	1.33200	70.663	21.0
7	0	0	4	1.23700	77.030	2.0
8	1	1	2	1.17290	82.105	23.0
9	2	0	0	1.15380	83.767	5.0
10	2	0	1	1.12360	86.560	17.0
11	1	0	4	1.09010	89.923	3.0
12	2	0	2	1.04560	94.903	5.0
13	2	0	3	0.94540	109.133	8.0
14	1	0	5	0.90930	115.803	6.0
15	1	1	4	0.90640	116.390	11.0
16	2	1	0	0.87220	124.054	5.0
17	2	1	1	0.85890	127.493	9.0
18	2	0	4	0.84370	131.847	2.0
19	0	0	6	0.82450	138.219	1.0
20	2	1	2	0.82250	138.955	9.0

2) ZnO, JCPDS file number 36-1451

Crystal system	:	Hexagonal
Space group	:	P63mc
Space group number	:	186
A	:	3.2498
B	:	3.2498
C	:	5.2066
Alpha	:	90.0000
Beta	:	90.0000
Gamma	:	120.0000
Volume of cell (10^6 pm^3)	:	47.62
Z	:	2.00

Peak list

No.	h	k	l	d [A]	2Theta[deg]	I [%]
1	1	0	0	2.81430	31.770	57.0
2	0	0	2	2.60332	34.422	44.0
3	1	0	1	2.47592	36.253	100.0
4	1	0	2	1.91114	47.539	23.0
5	1	1	0	1.62472	56.603	32.0
6	1	0	3	1.47712	62.864	29.0
7	2	0	0	1.40715	66.380	4.0
8	1	1	2	1.37818	67.963	23.0
9	2	0	1	1.35825	69.100	11.0
10	0	0	4	1.30174	72.562	2.0
11	2	0	2	1.23801	76.955	4.0
12	1	0	4	1.18162	81.370	1.0
13	2	0	3	1.09312	89.607	7.0
14	2	1	0	1.06384	92.784	3.0
15	2	1	1	1.04226	95.304	6.0
16	1	1	4	1.01595	98.613	4.0
17	2	1	2	0.98464	102.946	2.0

3) Cu, JCPDS file number 02-1225

Crystal system	:	Cubic
Space group	:	Fm3m
Space group number	:	225
A	:	3.6070
B	:	3.6070
C	:	3.6070
Alpha	:	90.0000
Beta	:	90.0000
Gamma	:	90.0000
Measured density (g/cm^3)	:	8.95
Volume of cell (10^6 pm^3)	:	46.93
Z	:	4.00

Peak list

No.	h	k	l	d [A]	2Theta[deg]	I [%]
1	1	1	1	2.08000	43.473	100.0
2	2	0	0	1.81000	50.375	80.0
3	2	2	0	1.28000	73.997	80.0
4	3	1	1	1.09000	89.934	80.0
5	2	2	2	1.04000	95.578	50.0
6	4	0	0	0.90000	117.716	20.0
7	3	3	1	0.83000	136.273	40.0
8	4	2	0	0.81000	143.974	40.0

4) CuO, JCPDS file number 41-0254

Crystal system	:	Monoclinic
Space group	:	C2/c
Space group number	:	15
a	:	4.6850
b	:	3.4230
c	:	5.1320
Alpha	:	90.0000
Beta	:	99.5200
Gamma	:	90.0000
Calculated density (g/cm^3)	:	6.51
Measured density (g/cm^3)	:	6.45
Volume of cell (10^6 pm^3)	:	81.17
Z	:	4.00

Peak list

No.	h	k	l	d [A]	2Theta[deg]	I [%]
1	1	1	0	2.75200	32.509	8.0
2	0	0	2	2.53100	35.438	60.0
3	-1	1	1	2.52400	35.539	100.0
4	1	1	1	2.32300	38.731	100.0
5	2	0	0	2.31100	38.941	100.0
6	-1	1	2	1.96080	46.264	3.0
7	-2	0	2	1.86670	48.743	25.0
8	0	2	0	1.71240	53.466	7.0
9	2	0	2	1.58110	58.312	12.0
10	-1	1	3	1.50550	61.549	16.0
11	0	2	2	1.41770	65.823	12.0
12	-3	1	1	1.40910	66.276	14.0
13	1	1	3	1.37870	67.934	9.0
14	2	2	0	1.37490	68.147	14.0
15	3	1	1	1.30370	72.436	6.0

APPENDIX B

PUBLICATIONS

Available online at www.sciencedirect.com

SciVerse ScienceDirect

Ceramics International 39 (2013) S501–S505

CERAMICS INTERNATIONAL

www.elsevier.com/locate/ceramint

Growth of hexagonal prism ZnO nanorods on Zn substrates by hydrothermal method and their photoluminescence

Nuengruethai Ekthammathat[a], Titipun Thongtem[a,*], Anukorn Phuruangrat[b,**], Somchai Thongtem[c]

[a]Department of Chemistry, Faculty of Science, Chiang Mai University, Chiang Mai 50200, Thailand
[b]Department of Materials Science and Technology, Faculty of Science, Prince of Songkla University, Hat Yai, Songkhla 90112, Thailand
[c]Department of Physics and Materials Science, Faculty of Science, Chiang Mai University, Chiang Mai 50200, Thailand

Available online 16 October 2012

Abstract

Hexagonal prism ZnO nanorods were successfully grown on Zn substrates by the 120 °C and 24 h hydrothermal reaction of the solutions with pH of 9–12. Results from XRD, SEM, TEM, SAED and HRTEM showed that the as-synthesized products were wurtzite ZnO with the shape of hexagonal prism nanorods grown along the [0 0 1] direction with smooth prismatic side planes. The PL spectra showed strong emission band at 543 nm in the green-yellow region due to the recombination of electrons trapped in singly ionized oxygen vacancies and photoexcited holes. This facile, reproducible and effective low-cost approach is promising for the future large-scale synthesis of wurtzite ZnO nanostructures for different applications in nanotechnology.

Keywords: B. Electron microscopy; B. X-ray methods; D. ZnO; E. Functional applications

1. Introduction

One dimensional (1D) nanostructured materials are usually synthesized by bottom-up directional growth process and are able to be applied in different areas such as transistors, UV light emitters, light emitting diodes, solar cells and gas sensors. Their properties are sensitively influenced by both shape and size, and are of fundamental and technological interests. Thus the development of synthetic method and understanding their formation mechanism are important in nanoscience and nanotechnology [1,2].

Zinc oxide (ZnO) is one of the important semiconductors with 3.37 eV direct band gap at room temperature and large 60 meV exciton binding energy. It is a promising material for efficient emission by low excitation energy at room temperature. Thus ZnO has been recognized as a valuable photonic material in the UV-blue region [1–3]. It is a bio-safe and biocompatible material, and is able to be directly used as a biomedical material with no further coatings [3].

Various methods have been used to synthesize 1D ZnO nanostructures: chemical bath deposition [4], chemical solution [5], sol–gel [6] and chemical vapor deposition (CVD) [7]. However, most of them generally involve two steps: depositing or spin coating of ZnO nanoparticles on substrates to form films of ZnO crystal seeds, and followed by growing of ZnO nanorod arrays on the seed coated substrate in an aqueous solution containing zinc ions [8]. In the present research, hexagonal prism ZnO nanorods were successfully grown on Zn substrates by low temperature hydrothermal reaction. The effect of pH on the formation of hexagonal prism ZnO nanorods on Zn substrates and a possible growth mechanism were proposed and discussed in detail.

*Corresponding author. Tel.: +66 53 943344; fax: +66 53 892277.
**Corresponding author. Tel.: +66 74 288374; fax: +66 74 288395.
E-mail addresses: ttpthongtem@yahoo.com (T. Thongtem), phuruangrat@hotmail.com (A. Phuruangrat).

0272-8842/$ - see front matter © 2012 Elsevier Ltd and Techna Group S.r.l. All rights reserved.
http://dx.doi.org/10.1016/j.ceramint.2012.10.122

2. Experiment

All reagents of this experiment were analytical grade and used without further purification. The hexagonal prism

ZnO nanorods were grown on Zn substrates or foils in sequence as follows. Several of 15 × 15 × 0.25 mm Zn substrates were carefully cleaned with deionized water and absolute alcohol in an ultrasound bath, respectively. They were put in NaOH aqueous solutions with the pH of 9–12. Each of the solutions and zinc substrates was transferred into Teflon-lined stainless steel autoclaves of 50 ml capacities. The autoclaves were tightly closed, heated at 120 °C in a laboratory electric oven for 24 h, and naturally cooled to room temperature. The zinc substrates were thoroughly washed by deionized water several times, and dried at 70 °C by an electric oven for 12 h for further characterization.

3. Results and discussion

Fig. 1 shows XRD patterns of the as-grown ZnO crystals on Zn substrates synthesized by hydrothermal reaction at 120 °C for 24 h in the solutions with different pH values. Before hydrothermal processing, all diffraction peaks of the substrates could be indexed as pure hexagonal Zn structure of the JCPDS no 04-0831 [9]. Upon hydrothermal processing at 120 °C for 24 h, wurtzite structured ZnO phase of the JCPDS no 36-1451 [9], and those marked with hexagonal Zn of the JCPDS no 04-0831 [9] were detected. It should be noted that the diffraction peaks of the as-synthesized ZnO were strong and sharp, specified as well crystallized products. Preferential orientation of the as-synthesized 1D nanostructured ZnO was determined from peak intensity of the as-synthesized products by comparing with that of the standard bulk. For the as-synthesized ZnO product, intensity of the (0 0 2) peak was higher than that of the (1 0 1) peak. But for the standard bulk ZnO, the (1 0 1) peak is the highest. This could be related to the preferential orientation and alignment of the as-synthesized ZnO crystal on Zn substrate. It was believed that the preferential orientation of ZnO grew along the *c* direction on the Zn substrate [10,11].

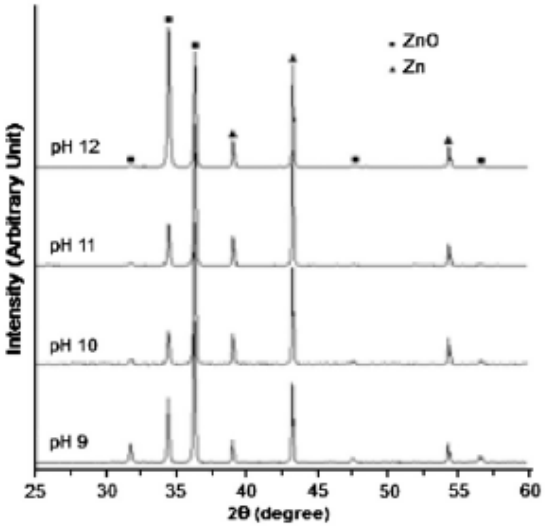

Fig. 1. XRD patterns of ZnO synthesized in the solutions of different pH values by the 120 °C and 24 h hydrothermal reaction.

The extent of *c* orientation of the as-synthesized ZnO crystals was explained by the relative texture coefficient (RTC) [12]. For random crystallographic orientation, RTC of ZnO is 0.5. In this research, RTC at (0 0 2) peak is 0.74, which supported the preferential orientation of the as-synthesized ZnO crystals grew along the [0 0 1] direction on the Zn substrate.

Morphologies of the as-synthesized ZnO products grown on Zn substrates were observed by SEM (Fig. 2). It showed that the product morphologies gradually developed from nanoparticles to nanorods, controlled by the pH of the solution. At pH 9, the surface of the zinc substrate was uniformly covered with ZnO nanoparticles. ZnO nanoparticles began to grow as ZnO nanorods at the pH 10. Upon increasing the pH of the solution to 12, the Zn substrate was densely covered with 1 μm long ZnO nanorods with 100–500 nm in diameters. The high-magnification of SEM image (inserted in Fig. 2d) revealed that ZnO crystals were hexagonal prismatic columns of well-resolved edges and corners with smooth faces. The angles between the two adjacent faces of individual hexagonal nanorods were 120°.

More detail of the product morphologies was investigated by TEM. The general TEM images, HRTEM image and SAED pattern of the as-synthesized ZnO nanorods at the pH 12 are shown in Fig. 3. TEM images show hexagonal columnar ZnO nanostructures with diameter range of 20–80 nm and lengths of several hundred nanometers. The corresponding SAED pattern indicates that each ZnO nanocolumn was single crystal. It can be indexed to be the hexagonal ZnO phase, in accordance with the above XRD analysis. The HRTEM image shows interplanar space of about 0.28 nm, corresponding to the fringe of (1 0 0) ZnO plane, specified as the single crystal with the preferential growth in the [0 0 1] direction. SAED and HRTEM analysis confirmed that hexagonal prism ZnO single crystals grew along the [0 0 1] direction [3,6]. The formation of hexagonal ZnO nanorods was attributed to the difference in growth rate of the prominent crystalline facets with low surface energies during the growth of crystal. The surface energies of different hexagonal ZnO facets of the (0 0 0 1), (10–11), (10–10) planes are −2.8102, −2.1067 and −2.0013 kJ/mol, respectively. Therefore, the growth rates of the ZnO crystals in different planes are in sequence as follows: (0 0 0 1) > (10–11) > (10–10). Growth rate of the (0 0 0 1) plane was the most rapid leading to the sharp tips at the end of the nanorods. Growth rate of the (10–10) plane is at the slowest, and that of the (10–11) plane in the middle; therefore, they remained to form the hexagonal prism ZnO nanorods [8,13,14].

In general, size and shape of the products are controlled by the competition between crystalline nucleation and

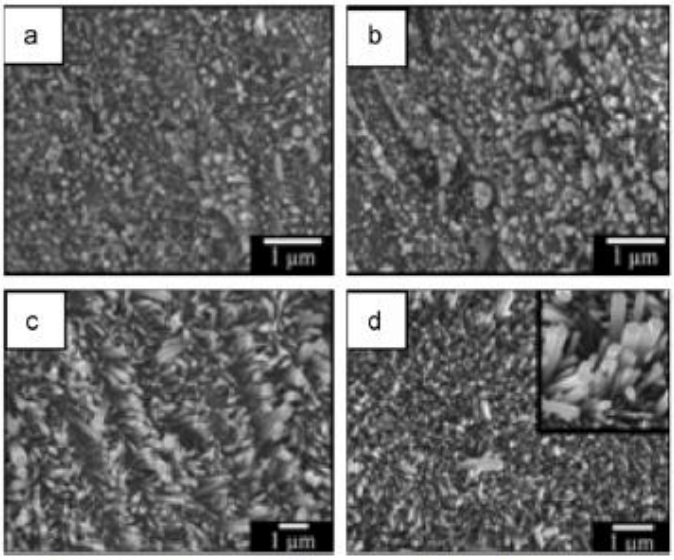

Fig. 2. SEM images of ZnO synthesized in the solutions with the pH of (a–d) 9, 10, 11 and 12 by the 120 °C and 24 h hydrothermal reaction.

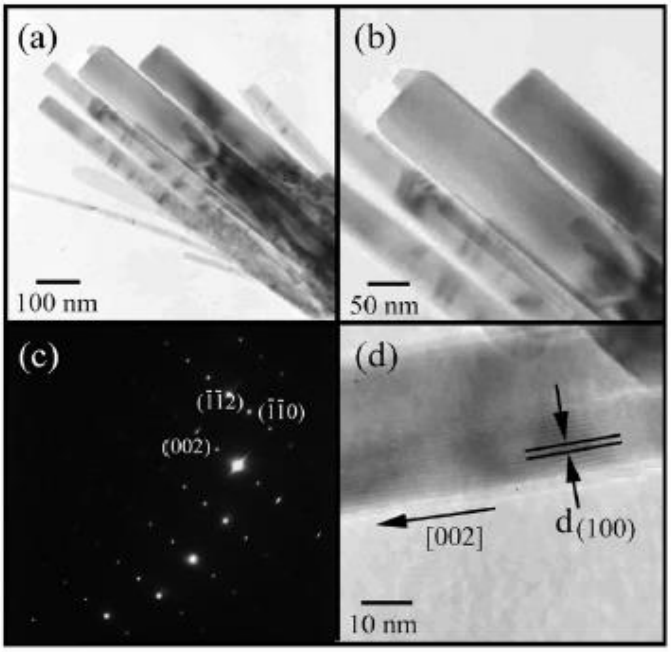

Fig. 3. (a, b) TEM images, (c) SAED pattern, and (d) HRTEM image of hexagonal ZnO nanorods synthesized in the solution with the pH 12 by the 120 °C and 24 h hydrothermal reaction.

growth, determined by the inherent crystal structure and the chemical potential of the precursor solution. For the nucleation rate of more than the growth rate, the crystals are small and low aspect ratio, with a large number of crystals. Contrarily, they are large, high aspect ratio and small number. Although the crystal growth is mainly determined by the intrinsic structure, it is affected by the external conditions such as pH, saturation and temperature.

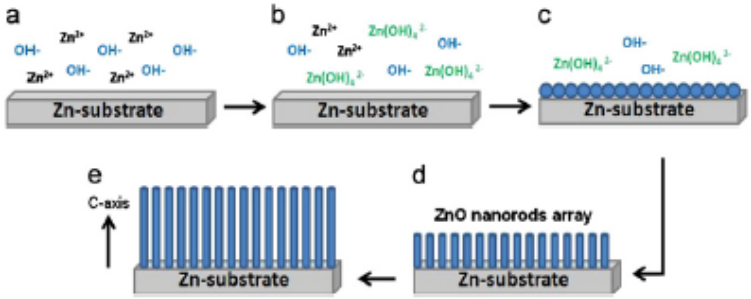

Fig. 4. Schematic diagram of a possible growth mechanism of hexagonal prism ZnO nanorods on Zn substrates.

In this work, pH of the solution was considered to play an important role in the formation of hexagonal prism ZnO nanorods [15,16]. Fig. 4 shows the schematic diagram of a possible growth mechanism of hexagonal prism ZnO nanorods grown on Zn substrate, simply explained in three basic steps. First, Zn substrate was dissolved in basic solution and Zn^{2+} ions formed. Second, $[Zn(OH)_4]^{2-}$ complex ions formed to create multiple nuclei on the zinc substrate. Third, homoepitaxial growth of nuclei proceeded as hexagonal prism ZnO nanorods by the 120 °C and 24 h hydrothermal reaction [8].

By continuously increasing the pH of the solution, a large number of ions were produced. This led the system in forming a supersaturated solution, which favored the formation of hexagonal prism ZnO nanorods. Hence, the facile growth of hexagonal prism ZnO nanorods on Zn substrates was attributed by the alkaline solution with very high concentration of hydroxide anions [8].

The room-temperature PL spectra of hexagonal ZnO (Fig. 5) were measured using 215 nm excitation wavelength. They show the same emission broad band at 510–640 nm with a strong band at 543 nm, corresponding to the green-yellow emission due to the recombination of electrons trapped at singly charged oxygen vacancies and photogenerated holes [17,18]. The emission became weakened by the desorption of OH^- groups on the surfaces of ZnO nanorods.

In general, two emissions were detected on ZnO nanorods: UV range caused by the recombination of electrons in conduction band and holes in valence band relating to band gap, and visible range by surface defects of crystals. Different rationalizations were caused by the change in PL of 1D ZnO nanostructures. The UV emission intensity is the maximum, when the 1D ZnO nanostructures have an orientation along the *c*-axis, and increases as the crystallite size increases. Meanwhile, surface defects, interstitial defects, and the adsorption of impurities on the surfaces of the nanorods can lead to different emissions in the visible range. Among the different defects are oxygen vacancy, zinc vacancy, oxygen interstitial, zinc interstitial and antisite oxygen. Oxygen vacancy is at the most to be mentioned. In general, visible emission is caused by the recombination of electrons trapped in singly charged

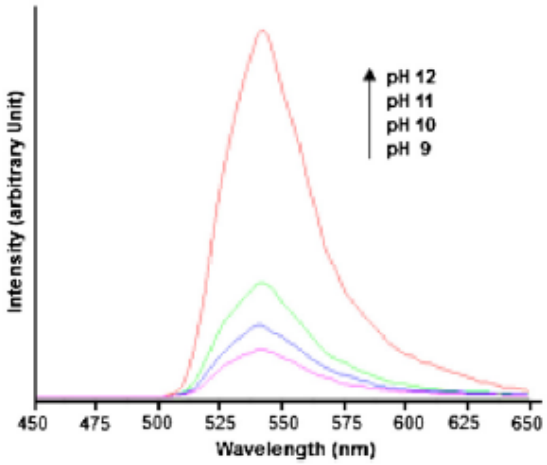

Fig. 5. PL spectra of ZnO synthesized by the 120 °C and 24 h hydrothermal reaction.

oxygen vacancies and photogenerated holes. Sometimes the photogenerated holes are first trapped on the product surface, diffused into the bulk, and subsequently combined with electrons trapped at the singly charged oxygen vacancies to form doubly charged oxygen vacancies. The recombination of holes at doubly charged oxygen vacancies and electrons in conduction band leads to the emission of visible spectrum. Considering the green emission, it is known to be the recombination of photogenerated holes with electrons occupying intrinsic defects, such as singly charged oxygen vacancies and antisite oxygen atoms. The emission intensity is increased with the increase in the concentration of defects, including the band bending effect due to the chemisorption of oxygen and the crystal. The yellow emission is caused by the zinc interstitial atoms [19,20].

4. Conclusions

The good crystalline hexagonal prism ZnO nanorods with high density were synthesized on Zn substrates by the

120 °C and 24 h hydrothermal reaction without the use of any catalysts or additives. Phases of the products were investigated by XRD, specified as wurtzite hexagonal ZnO structure on Zn substrates. SEM and TEM images revealed the presence of the hexagonal prism ZnO nanorods, preferentially grown along the [0 0 1] direction. Room temperature PL spectra were sharp and strong with the green-yellow emission at 543 nm.

Acknowledgments

We wish to thank the Thailand's Office of the Higher Education Commission for providing financial support through the Human Resource Development Project in Science Achievement Scholarship of Thailand, the National Research Council of Thailand through the Research Program for Fiscal Year 2556, and the Graduate School of Chiang Mai University through the general support.

References

[1] S.J. Kim, H.H. Kim, J.B. Kwon, J.G. Lee, B.H. O, S.G. Lee, E.H. Lee, S.G. Park, Novel fabrication of various size ZnO nanorods using hydrothermal method, Microelectronic Engineering 87 (2010) 1534–1536.
[2] T. Ghoshal, S. Kar, J. Ghatak, S. Chaudhuri, ZnO nanocones: Solvothermal synthesis and photoluminescence properties, Materials Research Bulletin 43 (2008) 2228–2238.
[3] A. Umar, S.H. Kim, J.H. Kim, Y.B. Hahn, Structural and optical properties of ZnO nanostructures grown on silicon substrate by thermal evaporation process, Materials Letters 62 (2008) 167–171.
[4] G.Z. Jia, Y.F. Wang, J.H. Yao, Fabrication and strain investigation of ZnO nanorods on Si composing sol-gel and chemical bath deposition method, Journal of Physics and Chemistry of Solids 73 (2012) 495–498.
[5] J. Zhao, Z.G. Jin, T. Li, X.X. Liu, Nucleation and growth of ZnO nanorods on the ZnO-coated seed surface by solution chemical method, Journal of the European Ceramic Society 26 (2006) 2769–2775.
[6] K. Prabakar, H. Kim, Growth control of ZnO nanorod density by sol-gel method, Thin Solid Films 518 (2010) e136–e138.
[7] T. Hirate, S. Sasaki, W. Li, H. Miyashita, T. Kimpara, T. Satoh, Effects of laser-ablated impurity on aligned ZnO nanorods grown by chemical vapor deposition, Thin Solid Films 487 (2005) 35–39.
[8] D. Wang, C. Song, Z. Hu, W. Chen, X. Fu, Growth of ZnO prisms on self-source substrate, Materials Letters 61 (2007) 205–208.
[9] Powder Diffract. File, JCPDS-ICDD, 12 Campus Boulevard, Newtown Square, PA 19073-3273, U.S.A. (2001).
[10] L. Yang, J. Yang, D. Wang, Y. Zhang, Y. Wang, H. Liu, H. Fan, J. Lang, Photoluminescence and Raman analysis of ZnO nanowires deposited on Si(100) via vapor–liquid–solid process, Physica E 40 (2008) 920–923.
[11] Y.J. Gao, W.C. Zhang, X.L. Wu, Y. Xia, G.S. Huang, L.L. Xu, J.C. Shen, G.G. Siu, P.K. Chu, Hydrothermal self-assembling of ZnO nanorods into sphere-like superstructures and their optical characteristics, Applied Surface Science 255 (2008) 1982–1987.
[12] F. Li, Z. Li, F.J. Jin, Structural and luminescent properties of ZnO nanorods prepared from aqueous solution, Materials Letters 61 (2007) 1876–1880.
[13] C.W. Yao, H.P. Wu, M.Y. Ge, L. Yang, Y.W. Zeng, Y.W. Wang, J.Z. Jiang, Triangle-shape ZnO prepared by thermal decomposition, Materials Letters 61 (2007) 3416–3420.
[14] Z. Fang, K. Tang, G. Shen, D. Chen, R. Kong, S. Lei, Self-assembled ZnO 3D flowerlike nanostructures, Materials Letters 60 (2006) 2530–2533.
[15] J.H. Yang, J.H. Zheng, H.J. Zhai, L.L. Yang, J.H. Lang, M. Gao, Growth mechanism and optical properties of ZnO nanosheets by the hydrothermal method on Si substrates, Journal of Alloys and Compounds 481 (2009) 628–631.
[16] W.B. Hu, D.T. Tian, Y.Z. Mi, G.H. Nie, Y.M. Zhao, Z.L. Liu, K.L. Yao, Synthesis and characterization of In_2O_3 nanocube via a solvothermal-calcination route, Materials Chemistry and Physics 118 (2009) 277–280.
[17] H. Zhang, J. Feng, J. Wang, M. Zhang, Preparation of ZnO nanorods through wet chemical method, Materials Letters 61 (2007) 5202–5205.
[18] X. Wang, K. Huo, F. Zhang, Z. Hu, P.K. Chu, H. Tao, Q. Wu, Y. Hu, J. Zhu, Structural regulation and optical properties of one-dimensional ZnO nanomaterials in situ grown from and on brass substrates, Journal of Physical Chemistry C 113 (2009) 170–173.
[19] J. Lee, J. Chung, S. Lim, Improvement of optical properties of post-annealed ZnO nanorods, Physica E 42 (2010) 2143–2146.
[20] L. Zhang, L. Yin, C. Wang, N. Lun, Y. Qi, D. Xiang, Origin of visible photoluminescence of ZnO quantum dots: Defect-dependent and size-dependent, Journal of Physical Chemistry C 114 (2010) 9651–9658.

Superlattices and Microstructures 53 (2013) 195–203

Contents lists available at SciVerse ScienceDirect

Superlattices and Microstructures

journal homepage: www.elsevier.com/locate/superlattices

Characterization of ZnO flowers of hexagonal prisms with planar and hexagonal pyramid tips grown on Zn substrates by a hydrothermal process

Nuengruethai Ekthammathat [a], Titipun Thongtem [a,d,*], Anukorn Phuruangrat [b,*], Somchai Thongtem [c,d]

[a] Department of Chemistry, Faculty of Science, Chiang Mai University, Chiang Mai 50200, Thailand
[b] Department of Materials Science and Technology, Faculty of Science, Prince of Songkla University, Hat Yai, Songkhla 90112, Thailand
[c] Department of Physics and Materials Science, Faculty of Science, Chiang Mai University, Chiang Mai 50200, Thailand
[d] Materials Science Research Center, Faculty of Science, Chiang Mai University, Chiang Mai 50200, Thailand

ARTICLE INFO

Article history:
Received 20 June 2012
Received in revised form 14 October 2012
Accepted 15 October 2012
Available online 2 November 2012

Keywords:
ZnO flower-like structure
Hexagonal prisms
Hydrothermal method

ABSTRACT

Flower-like ZnO crystals on zinc substrates were synthesized by a simple hydrothermal method in different solutions containing 0.05, 0.10, 0.20, 0.30 and 0.40 g LiOH. X-ray diffraction (XRD), Fourier transform infrared (FTIR) spectroscopy, scanning electron microscopy (SEM), transmission electron microscopy (TEM) and selected area electron diffraction (SAED) showed that the products were wurtzite hexagonal ZnO flowers, composed of single crystalline hexagonal prisms grown along the [0001] direction with planar and hexagonal pyramid tips, including the Zn–O stretching vibration at 411.5 cm^{-1}. Photoluminescence (PL), excited by a 215 nm wavelength at room temperature, exhibited strong green emission at 543 nm.

1. Introduction

Since the discovery of carbon nanotubes by Iijima in 1991, one dimensional (1D) nanomaterials, such as nanowires, nanotubes, nanorods and nanoribbons are very attractive for a number of worldwide researchers due to their unique physical, chemical and electron-transport properties, which are

* Corresponding authors. Address: Department of Chemistry, Faculty of Science, Chiang Mai University, Chiang Mai 50200, Thailand. Tel.: +66 (0)53 943344; fax: +66 (0)53 892277 (T. Thongtem), tel.: +66 (0)74 288374; fax: +66 (0)74 288395 (A. Phuruangrat).
E-mail addresses: ttpthongtem@yahoo.com (T. Thongtem), phuruangrat@hotmail.com (A. Phuruangrat).

0749-6036/$ - see front matter © 2012 Elsevier Ltd. All rights reserved.
http://dx.doi.org/10.1016/j.spmi.2012.10.013

different from those of their corresponding bulks. They have widely potential applications in devices and interconnected integration in nanoelectronics and molecular electronics [1–4]. Zinc oxide with a 3.37 eV direct band gap and a 60 meV large exciton binding energy is an important semiconducting and piezoelectric material, which has novel photoelectric and electronic properties as well as its promising functionalities: catalytic, electric, optoelectronic and piezoelectric properties, solar cells, lasers and other nanodevices [2,5–8]. Thus considerable efforts have been directed towards the production of well-aligned 1D nanostructured ZnO on substrates with specific optoelectronic and field-emission characteristics. These 1D nanorods were densely populated materials, and promoted rapid and effective diffusion of electrons through them for lasers and solar cells [9].

Physical and chemical methods such as vapor-phase approaches including pulsed laser deposition (PLD) [10], thermal evaporation [11–13] and chemical vapor deposition (CVD) [14,15] were used to synthesize the 1D metal oxide nanostructures deposited on substrates. These methods require high temperature and low pressure which are generally complex and expensive. Recently, hydrothermal route has been developed to synthesize ordered metal oxide nanostructures on substrates: ZnO [2,5,8], TiO_2 [16,17], Fe_3O_4 [18], CuO [19,20] and SnO_2 [21,22], by low temperature processing for controlling morphologies and phases and for scaling up production for commercial possibilities.

In this research, flower-like clusters of ZnO hexagonal prisms with planar and hexagonal pyramid tips were synthesized on zinc substrates by a hydrothermal method. The room temperature photoluminescence (PL) spectra of the flower-like ZnO nanostructures exhibited the sharp strong green emissions, which supports high potential optical applications.

2. Experimental procedure

All chemicals for this research were analytical grade and used without further purification. The ZnO hexagonal prisms with planar and hexagonal pyramid tips were fabricated on Zn substrates by a hydrothermal process at relatively low temperature. Test coupons of $15 \times 15 \times 0.25$ mm Zn foils as Zn source and substrates were carefully cleaned in an ultrasound bath containing deionized water and alcohol. The test coupons in the 20 ml aqueous solutions containing 0.05, 0.10, 0.20, 0.30 and 0.40 g LiOH as OH^- source were hydrothermally processed in 30 ml Teflon-lined stainless steel autoclaves at 120 °C for 1–24 h in an electric oven and cooled them down to room temperature. In the end, the coupons were thoroughly rinsed by deionized water several times and ethanol, dried in an electric oven at 70 °C under its atmospheric chamber for further characterization.

Crystalline phases and degree of the as-synthesized nanostructured samples were analyzed by X-ray diffractometer (XRD, Philips X'Pert MPD) operating at 20 kV 15 mA and using Cu Kα line in 2θ of 20–60°. The morphology investigation was carried out by field emission scanning electron microscope (FE-SEM, JEOL JSM-6335F) operating at 35 kV, including transmission electron microscope (TEM, JEOL JEM-2010) and selected area electron diffractometer (SAED) operating at 200 kV. Fourier transform infrared (FTIR, Bruker Tensor 27) spectrometer was carried out in the range of 400–1200 cm^{-1} at room temperature. The ZnO pellets with 1 cm in diameter for FTIR testing were prepared by 40 times dilution with KBr and pressed by 10 Torr pressure. Their optical properties were studied by a spectrophotometer (LS50B Perkin Elmer) using 215 nm excitation wavelength at room temperature.

3. Results and discussion

Crystal structure and phase of the as-synthesized ZnO grown on Zn substrates were characterized by XRD, as shown by the XRD patterns of Fig. 1. The XRD patterns corresponded with the (1 0 0), (0 0 2), (1 0 1), (1 0 2) and (1 1 0) planes at $2\theta = 31.77°$, 34.45°, 36.30°, 47.53° and 56.06° for wurtzite hexagonal ZnO structure of the JCPDS no 36-1451, and the (1 0 0) (1 0 1) and (1 0 2) planes at $2\theta = 39.03°$, 43.26° and 54.33° for hexagonal Zn structure of the JCPDS no 04-0831 [23]. No other characteristic peaks of impurities were detected in these samples. The spectra are very sharp, implying the high crystalline degree of the as-synthesized ZnO phase on Zn substrates. It should be noted that the relatively strong intensity peaks reflected and diffracted from the (1 0 1) and (0 0 2) crystallographic planes of wurtzite

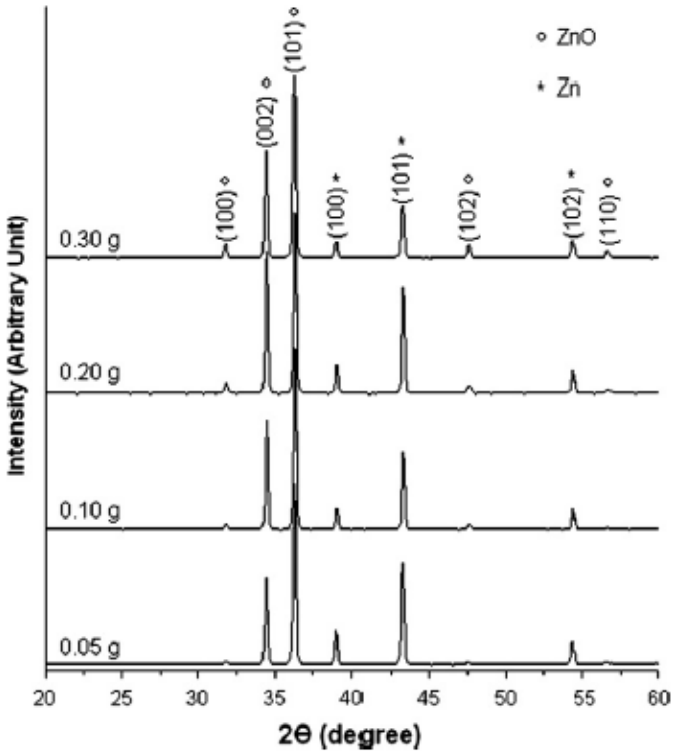

Fig. 1. XRD patterns of the as-synthesized ZnO phase on Zn substrates, hydrothermally synthesized in the solutions containing different contents of LiOH for 24 h.

hexagonal ZnO phase. Possibly, these ZnO unit cells preferentially grew along the [101] and [002] directions, in accordance with the XRD pattern reported by Pei et al. [24].

FTIR spectrum (Fig. 2) of the as-synthesized ZnO was recorded over the range of 400–1200 cm^{-1}. The main absorbance appeared at 411.5 cm^{-1} corresponding to the Zn–O stretching vibration of tetrahedral units [25], each of which was composed of four oxygen atoms with one zinc atom inside.

SEM images (Fig. 3) show the ZnO solid grown on Zn substrates by hydrothermal synthesis of the solution containing 0.10 g LiOH at 120 °C for different lengths of time. For 1 h, ZnO nanorod arrays were synthesized and uniformly covered the entire surface of zinc substrate. When the time was lengthened to 6 h, the ZnO solid was densely oriented hexagonal nanorods in large-scale uniform arrays with 50 nm in diameter grown on the Zn surface. By prolonging the reaction time to 18 h and 24 h, flower-like clusters of hexagonal prisms grown out of ZnO flower cores were more obviously detected. The ZnO individual hexagonal prism has 100 nm in diameter and 1–2 μm in length. High magnification SEM image (inserted in Fig. 3d) presents ZnO crystal shaped like a hexagonal prism with angles between the two adjacent edges of 120°. Each of them has planar tip on top. Obviously, the elongation of these crystals was the result of anisotropic growth of different crystal faces. The hexagonally prismatic shaped ZnO crystals originated by an axial growth of the hexagon normal to the (0001) crystallographic planes and directed along the *c*-axis of symmetry, including equatorial growth normal to the {10−10} family planes and radially pointed out of the *c*-axis [26,27]. Alternately, the individual ZnO hexagonal prism is surrounded by six ±(10−10), ±(1−100) and ±(01−10) prism planes with the acceleration of typical growth along the [0001] direction, leading to the formation of ZnO hexagonal prisms [26,28–30]. The solids appeared as high aspect ratio of hexagonal nanorods, identifying that the axial growth rate is faster than the equatorial growth rate [26].

Fig. 4 shows morphology development of the as-synthesized ZnO solids grown on Zn substrates by the 120 °C and 24 h hydrothermal reaction of the solutions containing different contents of LiOH. Clearly, the substrate was densely covered with ZnO hexagonal prisms of nanorods in the solution

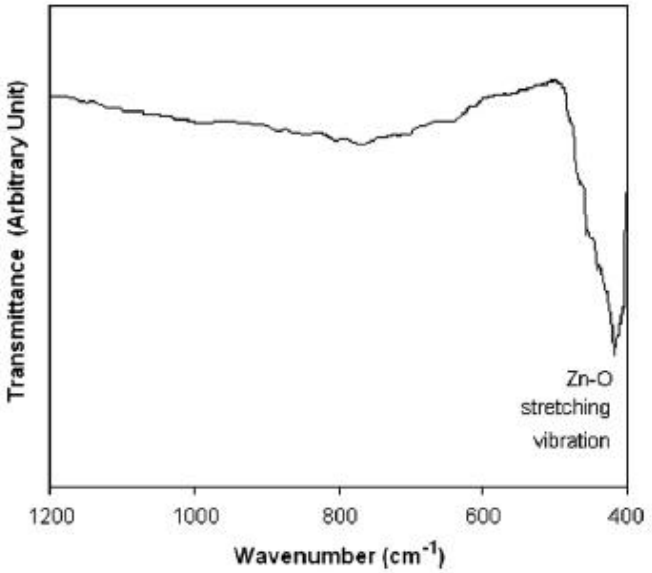

Fig. 2. FTIR spectrum of ZnO hydrothermally synthesized in the solution containing 0.30 g LiOH for 24 h.

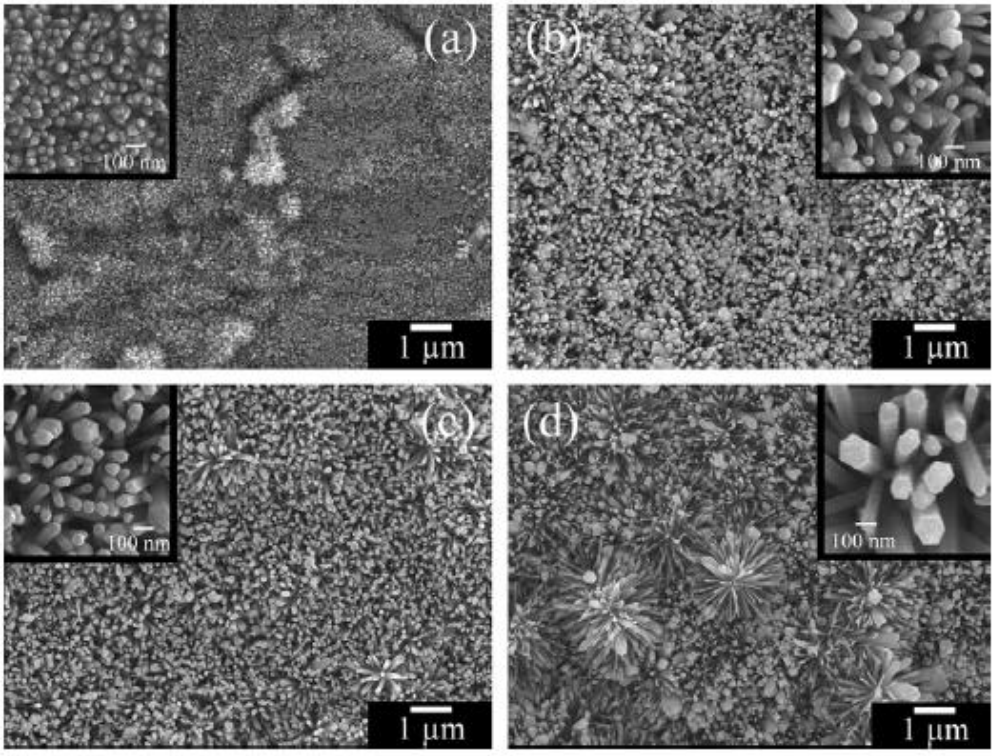

Fig. 3. SEM images of ZnO hydrothermally synthesized in the solution containing 0.10 g LiOH at 120 °C for (a–d) 1, 6, 18 and 24 h, respectively. High magnification images are shown as the insets.

containing 0.05 g LiOH. The ZnO nanorod arrays were about 1 μm long and 200 nm in diameters on average. At the current stage, ZnO flower-like clusters of nanorods shaped of hexagonal prism grown out of the ZnO cores were also detected on some areas of the substrate. Upon increasing the contents

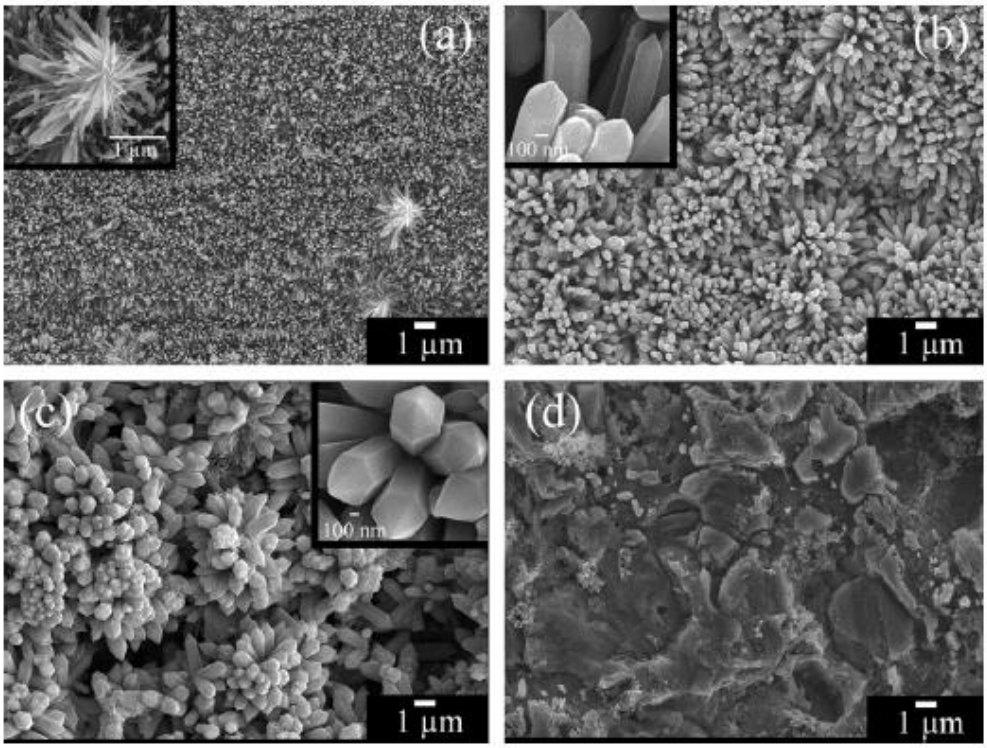

Fig. 4. SEM images of ZnO hydrothermally synthesized in the solutions containing (a–d) 0.05, 0.20, 0.30 and 0.40 g LiOH at 120 °C for 24 h, respectively. High magnification images are shown as the insets.

of LiOH from 0.05 g to 0.20 g and 0.30 g, the Zn substrates were fully covered with flower-like clusters of ZnO prisms. The top-view of these images was enlarged. They (inserted in Fig. 4b and c) appeared as ZnO hexagonal prisms of nanorods. These images indicated that an individual ZnO nanorod exhibits an obvious hexagonal prism with hexagonal pyramid-like sharp tip of well-defined crystallographic faces, pointing in different directions like a petal of flowers. In 0.40 g LiOH solution, the flower-like clusters were no longer synthesized and the Zn substrate was covered with irregular shape of ZnO agglomerates.

Further structural characterization of the ZnO flower-like hexagonal prism arrays with hexagonal pyramid sharp tips grown on the zinc substrates was studied by TEM. Typical TEM images (Fig. 5a and b) of ZnO hexagonal prisms with hexagonal pyramid sharp tips broken from a ZnO flower of hexagonal prisms present the assembly of several well-aligned nanorods with sharp tips, with their approximate lengths of 600 nm. Their diameters were 80 nm uniform along the entire lengths with very smooth surfaces. SAED pattern (Fig. 5c) of a single ZnO petal appeared as systematic bright spots, suggesting that the nanorod was single crystal. The pattern was identified as the [−1 1 0] electron beam projection on the ZnO petal [31]. The simulated pattern (Fig. 5d) [32] with a*, b* and c* lattice vectors in the [100], [010] and [001] directions are in systematic arrays, and in good accordance with the result obtained by current interpretation. Thus the product was really proved to be wurtzite ZnO, with the preferential growth of the ZnO nanorod along the [0001] direction [26,28,29]. To understand the characteristics of ZnO, it is necessary to study its growth mechanism. Wurtzite structured zinc oxide belongs to the P63mc space group with highly anisotropic structure along the *c*-axis. The (0001) plane terminated with Zn and the (000−1) plane with O. ZnO nanorods were easily synthesized by the nucleation and growth processes of the alternative arrangement of Zn and O atoms along the most favorable [0001] direction [26,33].

Fig. 6 shows a schematic diagram for a possible growth mechanism of ZnO hexagonal prisms with planar and hexagonal pyramid tips on Zn substrates. In a typical alkaline solution of synthetic

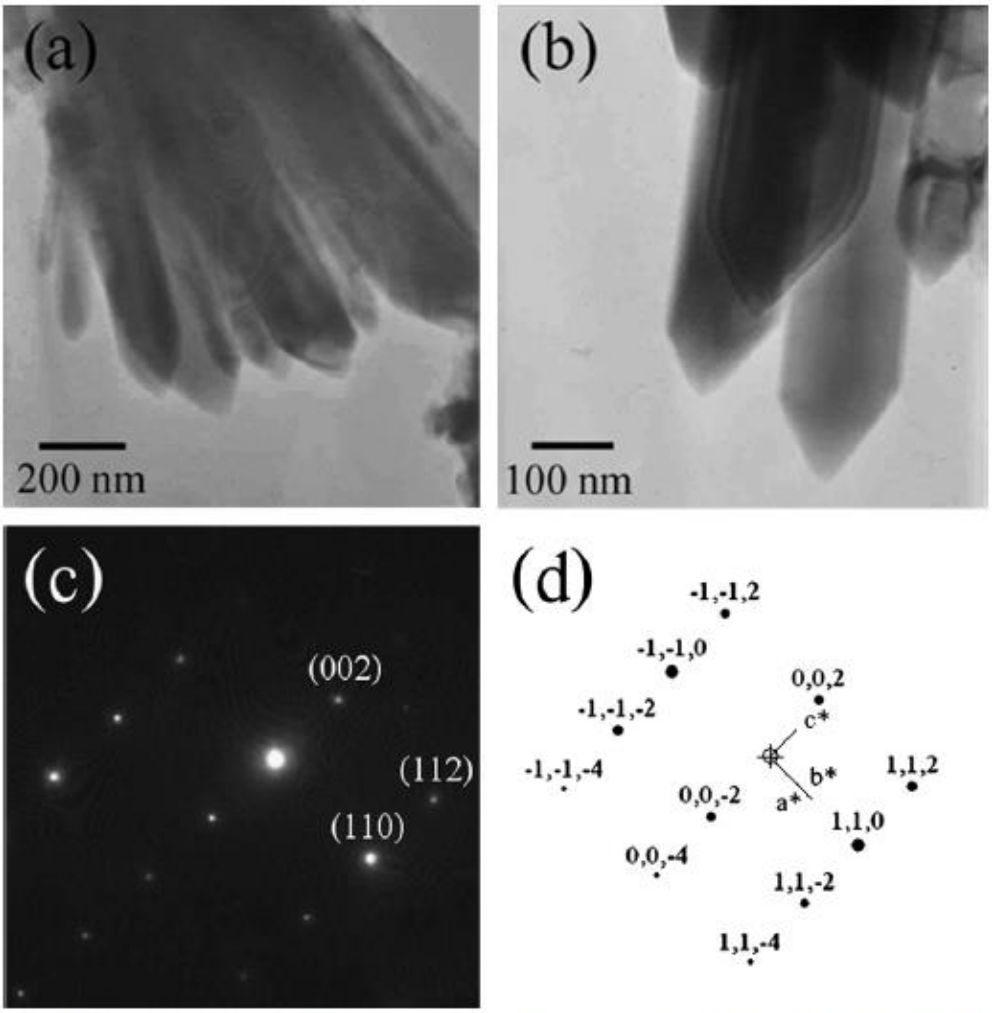

Fig. 5. (a, b) TEM images and (c) SAED pattern of hexagonal pyramid ZnO nanorods hydrothermally synthesized in the solution containing 0.30 g LiOH at 120 °C for 24 h, and (d) the simulation pattern of (c).

approach, $[Zn(OH)_4]^{2-}$ served as basic growth units for the formation of ZnO nuclei. In the present hydrothermal condition, Zn dissolved in the solution to form Zn^{2+} ions, which were further reacted with OH^- ions of LiOH to form $[Zn(OH)_4]^{2-}$. Subsequently, these $[Zn(OH)_4]^{2-}$ ions decomposed. ZnO molecular species were produced and nucleated as ZnO nuclei on Zn substrates. These ZnO nuclei grew to form hexagonal nanorod seeds. The hexagonal wurtzite ZnO with polar structure is hexagonal close packing of oxygen and zinc atoms in 3 m point group and P63mc space group with zinc atoms in tetrahedral sites. Thus, the crystal characteristics of wurtzite ZnO exhibit well defined crystallographic faces: (0001) base and nonpolar low symmetry (10–10) faces, with C_{6v} symmetry. In case of wurtzite ZnO polar crystal, each Zn^{2+} ion lies inside a tetrahedron of four oxygen ions. The Zn and O atoms are arranged alternatively along the *c*-axis such that the top face is the Zn-terminated (0001) plane and the bottom one the O-terminated (000–1) plane. The inherent asymmetry along the *c*-axis leads to the anisotropic growth of 1D ZnO crystallites. The formation of hexagonal prisms in the present study was attributed to the difference in growth rates of different crystal faces. The hydrothermal growth rates of different planes are as follows: (0001) > (10–11) > (10–10). The more rapid of the plane grows, the faster of its disappearance becomes. Therefore, the relative growth rate of these crystalline faces was determined the aspect ratio and final shape of the ZnO nanorods. The (0001) plane disappeared due to its most rapid growth rate leading to the sharp tip at the end of the *c*-axis. Growth rate of the (10–10) plane was at the slowest, therefore, the solids remained to form hexagonal prisms

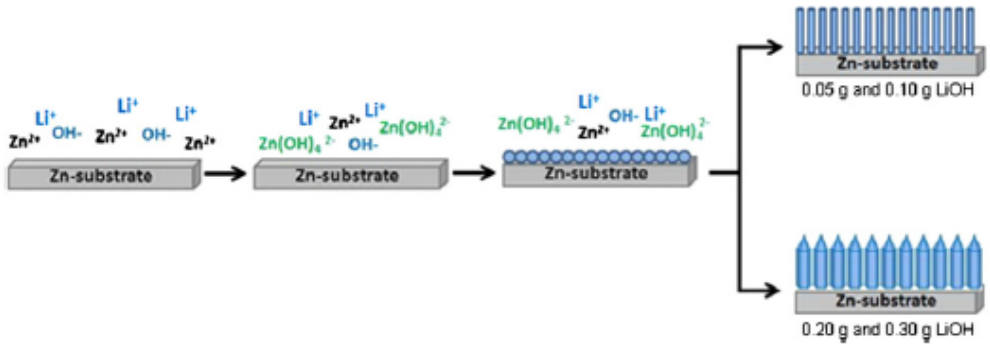

Fig. 6. Schematic diagram for a possible growth mechanism of ZnO hexagonal prisms with planar and hexagonal pyramid tips on Zn substrates.

with planar tips at lower pH (0.05 and 0.10 g LiOH), but the (10–11) plane remain to form hexagonal pyramid-like tips. However, the polar (0001) face is metastable and subjected to be etched at higher pH (0.20 and 0.30 g LiOH). Possibly, Zn atoms of the (0001) metastable polar face reacted with the OH^- ions, forming hydroxide species. The side faces of hexagonal prisms on the six ±[10−10], ±[1−100] and ±[01−10] symmetric directions were etched, remaining as hexagonal pyramid-like tips. Thus the one-dimensional growth continued to form hexagonal pyramid tips on top of ZnO nanorods [34,35].

The photoluminescence (PL) of ZnO was studied for its photonic applications. PL spectra (Fig. 7) of ZnO solids show the emission broad band at 505–625 nm in the visible range. They have the same strong green emission centered at 543 nm relating to different intrinsic defects originated during ZnO synthesis, but the exact mechanism is still ambiguous. There have been different proposed models to explain the emission from defects in ZnO crystal. The green emission at 542 nm originated from deep level associated with oxygen vacancies on outside walls of the ZnO nanorods [36,37]. Contrarily, the green emissions at 487 nm and 516 nm were believed to relate with oxygen vacancies, and the green–yellow emission at 574 nm to relate with oxygen vacancies [38]. In general, oxygen anions are so large that they are not able to reside in the interstitial sites of the ZnO solid synthesized by the 120 °C and 24 h hydrothermal method. The yellow–green emission at 573 nm is also known to be the presence of OH^- groups on the surface of ZnO nanorods, which were reduced by annealing the ZnO nanorods in oxygen atmosphere [39].

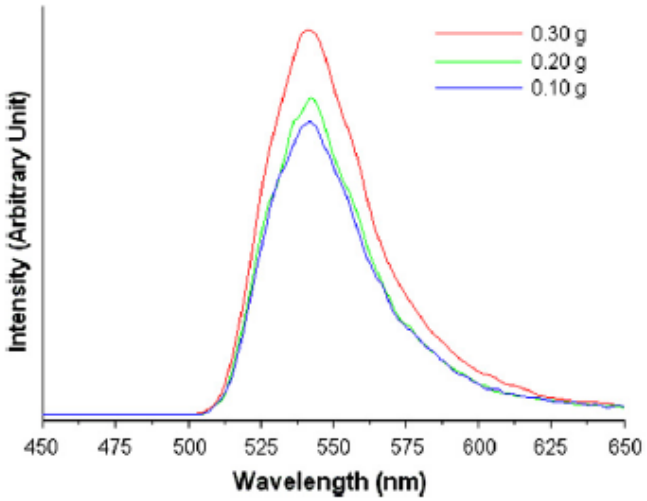

Fig. 7. PL spectra of ZnO hydrothermally synthesized in the solutions containing 0.10, 0.20 and 0.30 g of LiOH for 24 h.

4. Conclusions

Wurtzite ZnO solids were successfully synthesized on zinc substrates by a simple hydrothermal method at 120 °C for 24 h using 0.05–0.40 g LiOH. The phase, morphology and photoluminescence were characterized by X-ray diffraction, electron microscopy and spectrophotometry. In this research, the products were hexagonal wurtzite ZnO structure with the as-grown flower-like clusters composed of hexagonal prisms with planar and hexagonal pyramid tips on Zn substrates grown along the [0001] direction. Photoluminescence spectra exhibited strong green emission at 543 nm due to the presence of oxygen vacancies in the solid.

Acknowledgments

We wish to thank the Thailand's Office of the Higher Education Commission for providing financial support through the National Research University (NRU) Project for Chiang Mai University (CMU) and the Human Resource Development Project in Science Achievement Scholarship of Thailand (SAST), and the Thailand Research Fund (TRF) for providing financial support through the TRF Research Grant BRG5380020, including the Graduate School of CMU through the general support.

References

[1] S. Iijima, Helical microtubules of graphitic carbon, Nature 354 (1991) 56–58.
[2] Z. Li, X. Huang, J. Liu, Y. Li, G. Li, Morphology control and transition of ZnO nanorod arrays by a simple hydrothermal method, Mater. Lett. 62 (2008) 1503–1506.
[3] A. Phuruangrat, T. Thongtem, S. Thongtem, Characterisation of one-dimensional CdS nanorods synthesised by solvothermal method, J. Exp. Nanosci. 4 (2009) 47–54.
[4] T. Thongtem, C. Pilapong, J. Kavinchan, A. Phuruangrat, S. Thongtem, Microwave-assisted hydrothermal synthesis of Bi_2S_3 nanorods in flower-shaped bundles, J. Alloys Compd. 500 (2010) 195–199.
[5] C. Jia, X. Zhang, Y. Chen, Y. Su, Q. Zhou, M. Xin, Y. Lv, W. Kong, Liquid phase epitaxial growth and optical property of flower-like ZnO nanosheets on zinc foil, Appl. Surf. Sci. 254 (2008) 2331–2335.
[6] T. Thongtem, A. Phuruangrat, S. Thongtem, Characterization of nanostructured ZnO produced by microwave irradiation, Ceram. Int. 36 (2010) 257–262.
[7] A. Phuruangrat, T. Thongtem, S. Thongtem, Microwave-assisted synthesis of ZnO nanostructure flowers, Mater. Lett. 63 (2009) 1224–1226.
[8] Y. Tak, K. Yong, Controlled growth of well-aligned ZnO nanorod array using a novel solution method, J. Phys. Chem. B 109 (2005) 19263–19269.
[9] Z. Yang, C. Luan, W. Zhang, A. Liu, S. Tang, Fabrication and optical properties of ZnO nanostructured thin films via mechanical oscillation and hydrothermal method, Thin Solid Films 516 (2008) 5974–5980.
[10] K.A. Jeon, J.H. Kim, S.Y. Lee, Simple method for synthesis of silicon nanowire: pulsed laser deposition in furnace from p-Si wafer target, Prog. Solid State Chem. 33 (2005) 107–112.
[11] W. Lee, M.C. Jeong, J.M. Myoung, Catalyst-free growth of ZnO nanowires by metal-organic chemical vapor deposition (MOCVD) and thermal evaporation, Acta Mater. 52 (2004) 3949–3957.
[12] J.M. Wu, H.C. Shih, W.T. Wu, Y.K. Tseng, I.C. Chen, Thermal evaporation growth and the luminescence property of TiO_2 nanowires, J. Cryst. Growth 281 (2005) 384–390.
[13] S. Park, C. Hong, J. Kang, N. Cho, C. Lee, Growth of SnO_2 nanowires by thermal evaporation on Au-coated Si substrates, Curr. Appl. Phys. 9 (2009) S230–S233.
[14] F. Yu, D. Tang, K. Hai, Z. Luo, Y. Chen, X. He, Y. Peng, H. Yuan, D. Zhao, Y. Yang, Fabrication of SnO_2 one-dimensional nanosturctures with graded diameters by chemical vapor deposition method, J. Cryst. Growth 312 (2010) 220–225.
[15] R.R. Prabhakar, B. Varghese, W. Yuzhan, G. Xingyu, C.H. Sow, Carbon coated Nb_2O_5 nanowires as enhanced field emitters, Chem. Phys. Lett. 501 (2011) 431–436.
[16] F.D. Mai, W.L.W. Lee, J.L. Chang, S.C. Liu, C.W. Wu, C.C. Chen, Fabrication of porous TiO_2 film on Ti foil by hydrothermal process and its photocatalytic efficiency and mechanisms with ethyl violet dye, J. Hazard. Mater. 177 (2010) 864–875.
[17] Y. Su, S. Chen, N. Ma, X. Quan, H. Zhao, Photoelectrochemical characterization and application of direct-grown nanostructured anatase film via hydrothermal reactions, Separ. Purif. Technol. 68 (2009) 255–260.
[18] J. Chen, K. Huang, S. Liu, Hydrothermal preparation of a protective Fe_3O_4 film on Fe foil, Corr. Sci. 50 (2008) 1982–1986.
[19] Z.A. Jiang, J.T. Chen, J. Wang, R.F. Zhuo, D. Yan, F. Zhang, P.X. Yan, CuO nanosheets synthesized by hydrothermal process, Chin. Phys. Lett. 26 (2009) 086202.
[20] Y. Liu, Y. Chu, M. Li, L. Li, L. Dong, In situ synthesis and assembly of copper oxide nanocrystals on copper foil via a mild hydrothermal process, J. Mater. Chem. 16 (2006) 192–198.
[21] Q. Zhao, Z. Li, C. Wu, X. Bai, Y. Xie, Facile synthesis and optical property of SnO_2 flower-like architectures, J. Nanopart. Res. 8 (2006) 1065–1069.
[22] H.T. Chen, X.L. Wu, Y.Y. Zhang, J. Zhu, Y.C. Cheng, P.K. Chu, A novel hydrothermal route to synthesize solid SnO_2 nanospheres and their photoluminescence property, Appl. Phys. A 97 (2009) 581–585.
[23] Powder Diffract File, JCPDS-ICDD, 12 Campus Boulevard, Newtown Square, PA 19073-3273, USA, 2001.

[24] L.Z. Pei, H.S. Zhao, W. Tan, H.Y. Yu, Y.W. Chen, C.G. Fan, Q.F. Zhang, Hydrothermal oxidization preparation of ZnO nanorods on zinc substrate, Physica E 42 (2010) 1333–1337.
[25] S.K. Nandi, S. Chakraborty, M.K. Bera, C.K. Maiti, Structural and optical properties of ZnO films grown on silicon and their applications in MOS devices in conjunction with ZrO_2 as a gate dielectric, Bull. Mater. Sci. 30 (2007) 247–254.
[26] S.P. Garcia, S. Semancik, Controlling the morphology of zinc oxide nanorods crystallized from aqueous solutions: the effect of crystal growth modifiers on aspect ratio, Chem. Mater. 19 (2007) 4016–4022.
[27] C.X. Xu, G.P. Zhu, J. Kasim, S.T. Tan, Y. Yang, X. Li, Z.X. Shen, X.W. Sun, Spatial distribution of defect in ZnO nanodisks, Curr. Appl. Phys. 9 (2009) 573–576.
[28] C.X. Xu, X.W. Sun, Z.L. Dong, M.B. Yu, Zinc oxide nanodisk, Appl. Phys. Lett. 85 (2004) 3878–3880.
[29] M. Wang, S.H. Hahn, J.S. Kim, J.S. Chung, E.J. Kim, K.K. Koo, Solvent-controlled crystallization of zinc oxide nano(micro)disks, J. Cryst. Growth 310 (2008) 1213–1219.
[30] D. Chu, Y. Zeng, D. Jiang, Controlled growth and properties of Pb^{2+} doped ZnO nanodisks, Mater. Res. Bull. 42 (2007) 814–819.
[31] S. Jattukul, S. Thongtem, T. Thongtem, Morphology development of ZnO produced by sonothermal process, Ceram. Int. 37 (2011) 2055–2059.
[32] C. Boudias, D. Monceau, CaRIne Crystallography 3.1, DIVERGENT S.A., Centre de Transfert, 60200 Compiègne, France, 1989–1998.
[33] W. Peng, S. Qu, G. Cong, Z. Wang, Synthesis and structures of morphology-controlled ZnO nano- and microcrystals, Cryst. Growth Des. 6 (2006) 1518–1522.
[34] J.H. Yang, J.H. Zheng, H.J. Zhai, L.L. Yang, L. Liu, M. Gao, Solvothermal growth of highly oriented Wurtzite-structured ZnO nanotube arrays on zinc foil, Cryst. Res. Technol. 44 (2009) 619–623.
[35] D. Wang, C. Song, Controllable synthesis of ZnO nanorod and prism arrays in a large area, J. Phys. Chem. B 109 (2005) 12697–12700.
[36] H. Zhang, J. Feng, J. Wang, M. Zhang, Preparation of ZnO nanorods through wet chemical method, Mater. Lett. 61 (2007) 5202–5205.
[37] H. Gao, G. Fang, M. Wang, N. Liu, L. Yuan, C. Li, L. Ai, J. Zhang, C. Zhou, S. Wu, X. Zhao, The effect of growth conditions on the properties of ZnO nanorod dye-sensitized solar cells, Mater. Res. Bull. 43 (2008) 3345–3351.
[38] X. Wang, K. Huo, F. Zhang, Z. Hu, P.K. Chu, H. Tao, Q. Wu, Y. Hu, J. Zhu, Structural regulation and optical properties of one-dimensional ZnO nanomaterials in situ grown from and on brass substrates, J. Phys. Chem. C 113 (2009) 170–173.
[39] J. Lee, J. Chung, S. Lim, Improvement of optical properties of post-annealed ZnO nanorods, Physica E 42 (2010) 2143–2146.

Applied Surface Science 277 (2013) 211–217

Contents lists available at SciVerse ScienceDirect

Applied Surface Science

journal homepage: www.elsevier.com/locate/apsusc

Antimicrobial activities of CuO films deposited on Cu foils by solution chemistry

Nuengruethai Ekthammathat [a], Titipun Thongtem [a,c,*], Somchai Thongtem [b,c,**]

[a] Department of Chemistry, Faculty of Science, Chiang Mai University, Chiang Mai 50200, Thailand
[b] Department of Physics and Materials Science, Faculty of Science, Chiang Mai University, Chiang Mai 50200, Thailand
[c] Materials Science Research Center, Faculty of Science, Chiang Mai University, Chiang Mai 50200, Thailand

ARTICLE INFO

Article history:
Received 15 January 2013
Received in revised form 23 March 2013
Accepted 10 April 2013
Available online 17 April 2013

Keywords:
CuO thin films
Antimicrobial activity
Photoluminescence
X-ray techniques
UV–vis spectroscopy

ABSTRACT

Monoclinic CuO thin films on Cu foils were successfully synthesized by a simple wet chemical method in alkaline solution with the pH of 13 at room temperature for different lengths of time. The as-synthesized thin films were characterized by X-ray diffraction (XRD), Fourier transform infrared (FTIR) spectroscopy, scanning electron microscopy (SEM), transmission electron microscopy (TEM) and selected area electron diffraction (SAED). Formation mechanism of the phase and morphologies was also discussed according to the experimental results. In this research, assemblies of pure CuO nanospindles with different orientations containing in the thin film synthesized for 2 weeks with 400 nm and 413 nm violet emissions showed better antimicrobial activity against *S. aureus* than *E. coli*.

1. Introduction

Over the past decade, large-scale self-assemblies of meso-, micro- and nano-structured building components have received much attention in the synthesis of materials and fabrication of devices [1,2]. A number of self-assembly processes based on different driving mechanisms have become available. Among them, surface tension, capillary effect, and electric, magnetic and hydrophobic interactions have been utilized in various organization schemes [1]. Following the progress in assembly techniques, one-, two- and three-dimensional (1D, 2D, 3D) architectures have been achieved, leading to the possibility of applying a bottom-up approach in nanoscience and nanotechnology. Therefore, the ability to control, improve and manipulate the physical and chemical properties of nanostructures in the fabrication of efficient devices is one of the challenging issues facing materials scientists and engineers [1,3,4].

Different oxides of transition metals (iron, nickel, cobalt, zinc and copper) have a number of important applications. One of these is cupric oxide (CuO), a monoclinic crystal system which has been extensively studied. It is a p-type semiconducting material with a narrow band gap of 1.2 eV [5–8], and is a Mott insulator (3d transition metal monoxide) whose electronic structures cannot be simply described by conventional band theory [6]. CuO has been prepared by different methods: hydrothermal [1,5], solvothermal [2,9], thermal oxidation [6,10], sonochemical [11,12] and microwave irradiation [13,14]. These methods require an oxygen atmosphere to synthesize copper oxide, which can be oxidized with ease [15]. Furthermore, solution-phase synthesis at room temperature has been directed toward the fabrication of nanostructured CuO in the shapes of nanosheets [16], nanorods [17], nanoneedles and nanoflowers [18]. The method is considered to be one of the most promising synthetic processes, due to its high efficiency, low cost and excellent potential for high-quality production [16].

Many bacteria have been demonstrated to be sensitive to the antimicrobial properties of metals and metal oxides, carbon-based nanomaterials and surfactant-based nanoemulsions, including Ag, Al, Au, Cu, Zn, CuO, TiO_2, ZnO and C_{60} nanoparticles [19]. Cu nanoparticles have shown high affinity to amines and carboxyl groups on the surface of *Bacillus subtilis*, and hence are considered to have superior antibacterial activity. Copper oxide is cheaper than silver, easily miscible with polymers and possesses good chemical and physical stability [19]. These inorganic materials can be used in different forms: powders, coatings on cellulose fibers, nanocomposite coatings and thin films [20,21]. Antimicrobial coatings are of great interest for the protection of surfaces, since the survival of microorganisms on surfaces in the environment can lead to the

* Corresponding author at: Department of Chemistry, Faculty of Science, Chiang Mai University, Chiang Mai 50200, Thailand. Tel.: +66 053 943344; fax: +66 053 892277.
** Corresponding author at: Department of Physics and Materials Science, Faculty of Science, Chiang Mai University, Chiang Mai 50200, Thailand. Tel.: +66 053 941924; fax: +66 053 943445.
E-mail addresses: ttpthongtem@yahoo.com, ttpthongtem@gmail.com (T. Thongtem), schthongtem@yahoo.com (S. Thongtem).

0169-4332/$ – see front matter © 2013 Elsevier B.V. All rights reserved.
http://dx.doi.org/10.1016/j.apsusc.2013.04.027

spread of diseases. In addition, coatings are expected to have better safety and stability, while nanopowders may be hazardous to human health due to the risk of inhalation [20]. The antibacterial properties of metallic nanoparticles can be applied in a variety of fields such as medical treatment and devices, water treatment and food processing [15]. Therefore, the development of nanostructured coatings with antimicrobial properties is of prime importance [20].

In the present research, a simple and easy method was developed for the synthesis of nanostructured CuO thin films on Cu foils by a wet chemical method at room temperature without using any templates or seeds on top. The physiochemical, photoluminescent and antibacterial properties of the resulting CuO thin films were investigated.

2. Experimental procedure

2.1. Synthesis of solid films

All reagents in this experiment were of analytical grade and were used without further purification. CuO thin films were grown on Cu foils by the following sequence. A large piece of Cu foil with 0.25 mm thick was cut into several 15 mm × 15 mm test coupons, which were carefully cleaned with deionized water and absolute alcohol in an ultrasonic bath to remove surface impurities and oxide layers. Concurrently, an alkaline solution was prepared by adding of 10 M NaOH to deionized water until pH of the solution was 13. Then each of the Cu foils was separately immersed in the 10 ml alkaline solution at room temperature for 3–21 days to form copper oxide films on top. During immersion, color of the solutions changed from clear to light blue, which was attributed to dissolution of the copper foils. At the end of the process, the copper foils were thoroughly washed several times with deionized water and dried at 70 °C in an electric oven for 12 h.

2.2. Characterization

Crystallinity and phases of the products were characterized by an X-ray diffractometer (XRD, Philips X'Pert MPD) using a Cu Kα radiation at 45 kV and 35 mA in the range of 30–70°, surface morphologies by a field emission scanning electron microscope (FE-SEM, JEOL JSM-6335F) operating at 35 kV and a transmission electron microscope (TEM, JEOL JEM-2010) equipped with a selected area electron diffractometer (SAED) operating at 200 kV, atomic vibrations by a Fourier transform infrared spectrometer (FTIR, PerkinElmer RX Spectrophotometer) operating in the range of 400–2000 cm^{-1} at room temperature with a CuO tablet diluted with KBr for 40 times, and emission wavelengths by photoluminescence (PL, LS 50B PerkinElmer) using 330 nm excitation wavelength at room temperature.

2.3. Antibacterial testing

In this research, two kinds of bacteria – *Gram-positive* (*Staphylococcus aureus*) and *Gram-negative* (*Escherichia coli*) – were used to study the antibacterial activity of CuO thin films by an inhibition zone method. Both strains were transferred into flasks containing nutrient broth (NB) with an initial optical density (OD) of 0.1 at a 660 nm orange wavelength; and the bacteria were cultured at 37 °C in aerated conditions until reaching an OD of 0.3. Agar was then added to the flasks. Modified agar diffusion assays (testing disks) were used to determine the antibacterial activity of CuO thin films after 24 h incubation at 37 °C by the formation of clear zones around the copper foils.

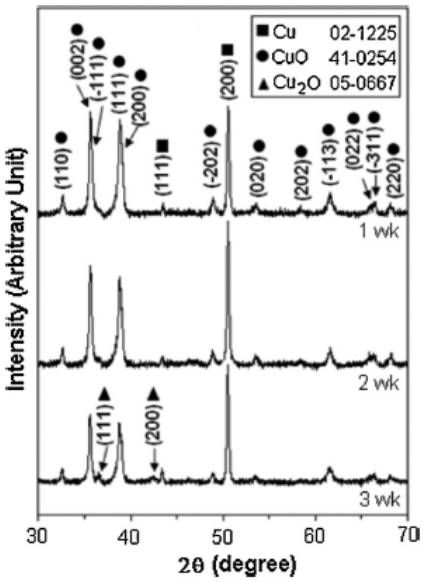

Fig. 1. XRD patterns of CuO thin films grown on Cu foils by wet chemical method at room temperature for 1, 2 and 3 weeks.

3. Results and discussion

3.1. XRD

XRD patterns of CuO films grown on copper foils for different lengths of time are shown in Fig. 1. All of the diffraction peaks were indexed and specified as monoclinic CuO (JCPDS No. 41-0254) with lattice constants a = 4.6850 Å, b = 3.4230 Å and c = 5.1320 Å, and Cu (JCPDS No. 02-1225) [22] after 1 and 2 weeks immersion of copper foils in the alkaline solution. It should be noted that the diffraction peaks of the as-synthesized CuO were strong and sharp, being specified as well-crystallized products. No other impurities were detected. The film became thickened with the increase in the length of time. Upon extending the reaction time to 3 weeks, Cu_2O (JCPDS No. 05-0667) [22] was also detected. This finding is attributed to the formation of Cu_2O on the foil, caused by an incomplete reaction at the film–foil interface. Thus the thickest pure CuO film synthesized for two weeks was used for further study. The thinner pure CuO and the mixed CuO–Cu_2O films on Cu foils were not appropriate for studying their antimicrobial properties.

3.2. FTIR

The FTIR transmittance spectrum (Fig. 2) of the CuO film on Cu foil synthesized for 2 weeks was recorded at room temperature. According to group theory calculation, CuO with the C_{2h}^6 space group and two molecules per primitive cell contribute the zone center normal modes: $\Gamma = 4A_u + 5B_u + A_g + 2B_g$, corresponding to six $3A_u + 3B_u$ IR active modes; three $A_u + 2B_u$ acoustic modes; and three $A_g + 2B_g$ Raman active modes [16]. The three characteristic IR peaks at 420, 508 and 609 cm^{-1} [4,16] are assigned as the A_u mode for the first, and $2B_u$ modes for the second and third [16]. The high-frequency modes at 609 cm^{-1} and 508 cm^{-1} correspond to Cu—O stretching along the [−1 0 1] and [1 0 1] directions, respectively [16]. No vibrations at 615–621 cm^{-1} of Cu_2O impurities were

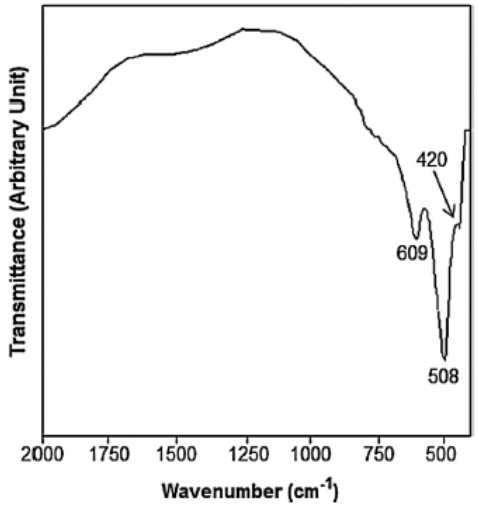

Fig. 2. FTIR spectrum of CuO thin film grown on Cu foil by wet chemical method at room temperature for 2 weeks.

detected [16,23]. This FTIR analysis confirmed that the solid film synthesized for 2 weeks was pure CuO phase.

3.3. SEM

Morphologies and particle sizes of the films grown on Cu foils at room temperature were characterized by scanning electron microscopy. SEM images (Fig. 3) show the gradual development of their morphologies and particle sizes, controlled by different lengths of reaction time and concentrations of hydroxyl ions. After 3, 5, 7 and 9 days synthesis (Fig. 3a–d), the copper foils were covered with films consisting of a number of particles with facets and angles. Particle size and film thickness were increased by prolonging the synthesis time. Particles as large as 1–1.5 μm were obtained after 9 days of synthesis. The films (Fig. 3e–i) were covered with assemblies of nanospindles with different orientations after synthesis for 12 days or longer. The sudden change of external surface morphologies from faceted and angled particles (Fig. 3a–d) to assemblies of nanospindles (Fig. 3e–i) was influenced by a decrease in the concentration of hydroxyl ions in the solutions (alkalinity effect), allowing nanospindles to form on top of the precursor particles. After 3 weeks synthesis, the external surface was covered with 1 μm wide and 2–3 μm long assemblies of nanospindles.

3.4. TEM and SAED

To further study the morphology and crystalline structure of CuO thin film, an assembly of nanospindles was characterized by TEM. Fig. 4a shows an assembly of nanospindles synthesized at room temperature for 2 weeks. The SAED pattern (Fig. 4b) indicated pure monoclinic CuO single crystal [22] with [0 0 −1] as the zone axis, which was in good accordance with the above XRD analysis. The simulated pattern [24] (Fig. 4c) with a^*, b^* and c^* reciprocal lattice vectors in the [1 0 0], [0 1 0] and [0 0 1] directions was in a systematic array, and in good accordance with that obtained by the interpretation. The crystal structure of monoclinic CuO phase was simulated using the atomic positions of Cu (0.25, 0.25, 0) and O (0, 0.5789, 0.25) [25], as shown in Fig. 4d. It belongs to the monoclinic crystal system, with C2/c space group. The copper atom is coordinated by 4 oxygen atoms in an approximately square planar configuration [25].

3.5. Formation mechanism

During initial stage of the synthesis, clean and fresh copper foils were separately immersed in 10 ml NaOH solutions (pH 13) at room temperature. Cu foils (copper sources) dissolved in the solutions as Cu^{2+} ions with electrons left behind. The oxidation rate was very fast, and the Cu^{2+} ions were continuously released into the solutions [18]. The released ions combined with hydroxyl ions to form $Cu(OH)_2$ precipitates (ppt) on top of the copper foils, which were transformed into CuO (solid films) after 12 h dehydration at 70 °C, in accordance with the most stable oxidation states of Cu^{2+} and O^{2-}. At high OH^- concentration, $[Cu(OH)_4]^{2-}$ complex ions could also form, which precipitated as $Cu(OH)_2$ and decomposed into CuO (solid films) by the dehydration process. Possibly, dissolved O_2 in the alkaline solution directly accepted the electrons, forming CuO (ppt). At this stage, the concentration of OH^- ions influences the nucleation and growth processes, such as the content of nuclei and growth units [7] and growth rate of different crystalline faces, thus leading to the formation of anisotropic particles [5].

$$Cu^0 \rightarrow Cu^{2+} + 2e^-$$

$$Cu^{2+} + 2OH^- \rightarrow Cu(OH)_2\,(ppt)$$

$$Cu(OH)_2 + 2OH^- \rightarrow [Cu(OH)_4]^{2-}\,(complexions)$$

$$2[Cu(OH)_4]^{2-} \rightarrow 2Cu(OH)_2\,(ppt) + 2H_2O + O_2 + 4e^-$$

$$Cu(OH)_2 \rightarrow CuO\,(solidfilms) + H_2O$$

$$O_2\,(dissolvingoxygeninsolution) + 4e^- \rightarrow 2O^{2-}$$

$$Cu^{2+} + O^{2-} \rightarrow CuO\,(ppt)$$

After a sufficient length of time, the oxidation rate slowed down; this was controlled by the diffusion rate of oxygen ions through the $Cu(OH)_2$ solid films coated on the copper foils. Ultimately, dissolving oxygen ions in the solutions diffused through $Cu(OH)_2$ films to the film–foil interfaces due to the concentration gradient. However, there was a deficiency of oxygen ions at the film–foil interfaces. Thus, the incomplete reaction process (due to deficient oxygen and rich copper) resulted in the formation of Cu_2O (solid) coating on the copper foils, in accordance with the oxidation states of 1+ for copper and 2− for oxygen.

$$Cu^0 \rightarrow Cu^{1+} + e^-$$

$$2Cu^{1+} + O^{2-} \rightarrow Cu_2O\,(solid)$$

The formation of solid films on copper foils is schematically shown in Fig. 5.

3.6. Photoluminescence

Photoluminescence (PL) spectroscopy was used to study the emission properties (Fig. 6) of the products. The electronic transition between the higher sub-levels of the conduction band and the Cu d-orbital of the valence band [23] led to three PL emissions after different lengths of reaction time. Emissions from CuO thin films synthesized for 1 and 2 weeks, respectively, appeared as violet luminescent bands at 400 nm (3.10 eV) and 413 nm (3.00 eV) with broad tails in the green spectral region [26]. Upon increasing the reaction time from 1 week to 2 weeks, the PL intensity

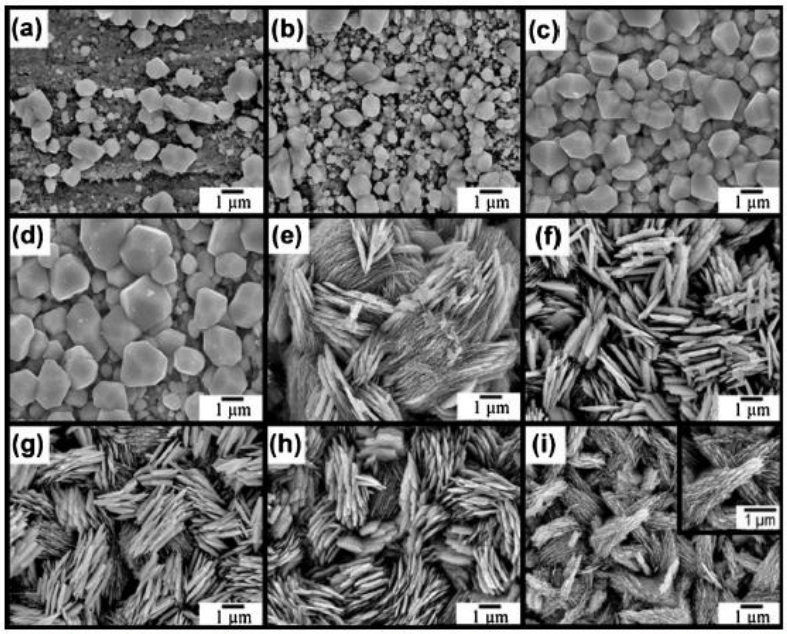

Fig. 3. SEM images of thin films grown on Cu foils by wet chemical method at room temperature for (a–i) 3, 5, 7, 9, 12, 14, 16, 19 and 21 days, respectively.

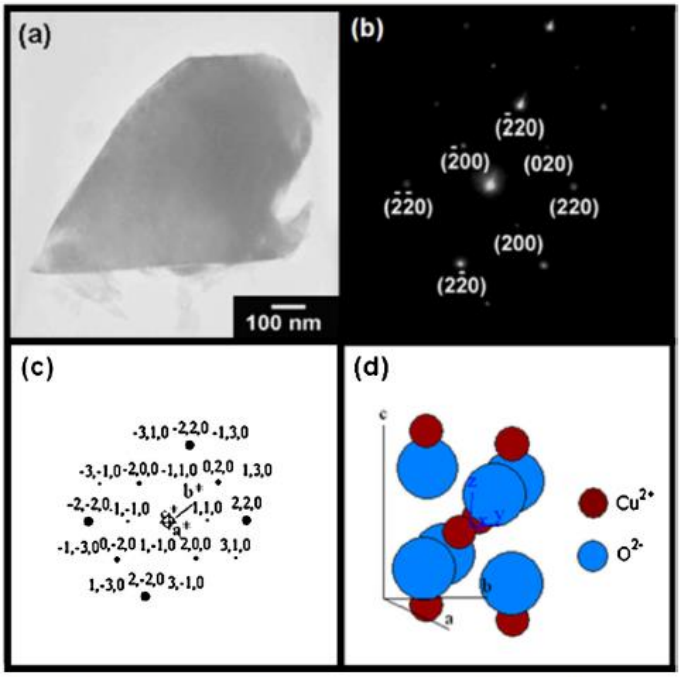

Fig. 4. (a) TEM image and (b) SAED pattern of an assembly of nanospindles grown on copper foil by wet chemical method at room temperature for 2 weeks. (c, d) The simulated pattern and unit cell of a spindle.

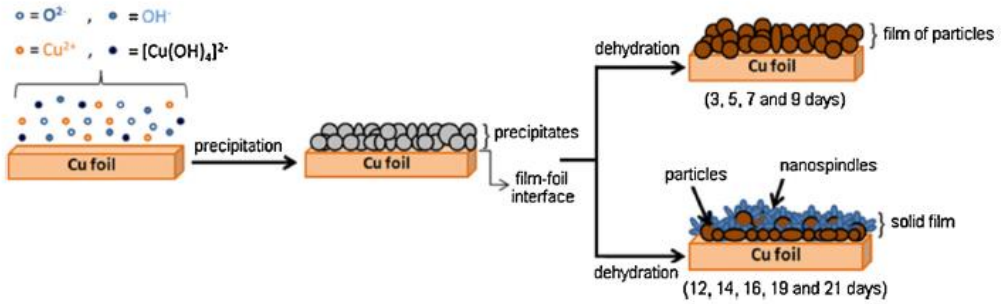

Fig. 5. Different stages for the formation of solid thin films on copper foils by wet chemical method at room temperature.

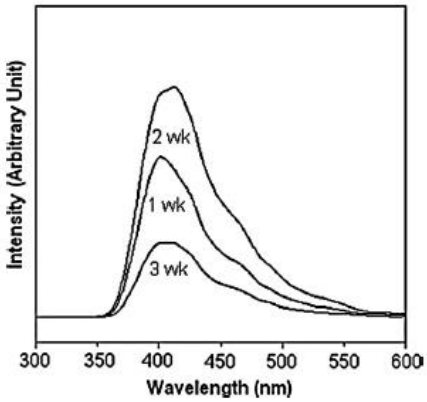

Fig. 6. PL spectra of thin films grown on Cu foils by wet chemical reactions at room temperature for 1, 2 and 3 weeks.

was strengthened. For 3 weeks synthesis, PL intensity was the lowest. The mixed phases of CuO and Cu_2O were likely to form some undesired defects inside, leading to the broadened and lowered peak. In this research, CuO thin film synthesized for 2 weeks was determined to be optimal for studying antimicrobial activity.

3.7. Antimicrobial activities

CuO thin film demonstrated antimicrobial activities against *Gram-positive* (*S. aureus*) and *Gram-negative* (*E. coli*) bacteria strains. The antimicrobial activities of CuO thin films were studied using the modified Kirby–Bauer method by observing an inhibition zone around the thin film [27]. In these tests, CuO thin films on Cu foils partially covered the NB agar disk. Bacteria with 0.3 OD were then sprayed on top. Before incubation (Fig. 7a and c), the CuO thin films did not show any significant antimicrobrial effects against *S. aureus* and *E. coli*. After 24 h incubation at 37 °C, bacterial growth in the NB agar was visualized (Fig. 7b and d); average diameters of the inhibition zones around the CuO thin films were measured as 25.17 mm for *S. aureus* and 22.50 mm for *E. coli*. Their different sensitivities appear to be related to the nature of their cell wall structures. *S. aureus* is composed of multiple layers of peptidoglycan

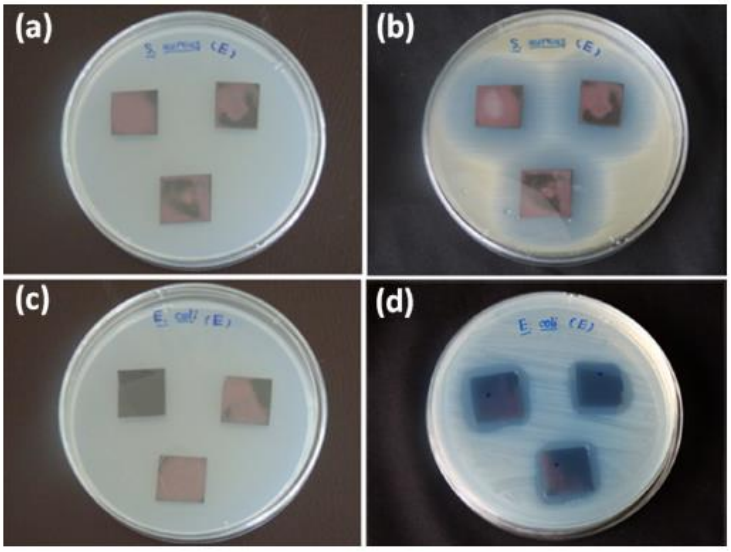

Fig. 7. Antibacterial activity of CuO thin films for (a, b) *S. aureus*, and (c, d) *E. coli*. (a, c) Before and (b, d) after 24 h incubation at 37 °C.

with numerous pores that were more susceptible to the intracellular transduction caused by the CuO thin film, leading to cell wall disruption. In contrast, the cell walls of *E. coli* are relatively thin, mainly consisting of peptidoglycan and outer layers of lipopolysaccharide, lipoprotein and phospholipids, which would be less prone to be attacked by the CuO thin film [28]. In summary, CuO thin film has higher antibacterial activity against *S. aureus* than *E. coli*.

Copper is a structural constituent of enzymes in many living microorganisms. Furthermore, free Cu^{2+} ions at high concentrations are able to produce hazardous effects by generating reactive oxygen species (ROS) such as $^{\bullet}O_2^-$, $^{\bullet}HO_2$, $^{\bullet}OH$ and H_2O_2 [3], which cause serious disruptions to amino acid synthesis and DNA [19]. The production of ROS by CuO in the environment of modified agar diffusion assays was achieved by the following sequence. During antimicrobial testing, bottom sides of the CuO films were in contacted with the NB agar disk. Thus the excitation process was dominantly influenced by ultraviolet radiation, especially by 320–400 nm wavelengths of UVA. In this research, O_2 molecules were reduced by excited electrons to form $^{\bullet}O_2^-$ superoxide anion radicals [3]. At the same time, H_2O molecules were decomposed into H^+ and OH^- by UVA-generated holes [29]. The $^{\bullet}O_2^-$ superoxide anion radicals reacted with H^+ to generate $^{\bullet}HO_2$ radicals, which collided with electrons to produce HO_2^- hydrogen peroxide anions. The HO_2^- hydrogen peroxide anions reacted with hydrogen ions to produce H_2O_2 molecules [29]. $^{\bullet}OH$ radicals could be synthesized by the collision of UVA-generated holes and H_2O molecules [30]. In the end, the generated ROS initially interacted with outer cell walls and further generated free radicals. The radicals penetrated the inner cell membranes which led to serious disruption of their internal contents; the cells became deformed and disorganized, causing leakage [3]. When the combination processes was not possible, electron–hole pairs could be recombined together to generate heat inside the CuO thin film. In summary, CuO thin film demonstrated excellent antibacterial performance, killing the bacteria by generating ROS to disrupt them. It should be noted that the cytotoxic activities of the Ti–Cu intermetallic thin films on Ti6Al4V alloy against *S. epidermidis* and *S. aureus* were influenced by copper releasing from the films. Titanium was used to increase hardness of the films and to improve adhesion of the films to the Ti6Al4V substrates [31]. Both Ti–Cu and CuO films can play the role in antimicrobial activities against bacteria. In case of Ti–Cu thin films, the antimicrobial activities were controlled by copper releasing from the films. But for the case of CuO thin films, they were controlled by the formation of ROS.

4. Conclusions

CuO thin films on Cu foils were successfully synthesized by a simple wet chemical method by emersion of the foils in the 10 ml alkaline (10 M NaOH) solution with the pH of 13 at room temperature for different lengths of time. For two weeks long, the Cu foil was covered with assemblies of nanospindles with different orientations of pure CuO on top. This film showed two strong violet emission intensities at 400 nm (3.10 eV) and 413 nm (3.00 eV) with broad tails in the green spectral region. Due to the UVA radiation, assemblies of pure CuO nanospindles film of the bottom side showed antimicrobial activity against *S. aureus* better than *E. coli* by generating reactive oxygen species (ROS) to disrupt them.

Acknowledgements

We wish to thank the Thailand's Office of the Higher Education Commission for providing financial support through the National Research University (NRU) Project and the Human Resource Development Project in Science Achievement Scholarship of Thailand (SAST), and the Graduate School of Chiang Mai University through a general support.

References

[1] Y. Liu, Y. Chu, M. Li, L. Li, L. Dong, In situ synthesis and assembly of copper oxide nanocrystals on copper foil via a mild hydrothermal process, Journal of Materials Chemistry 16 (2006) 192–198.
[2] W. Zhang, S. Ding, Z. Yang, A. Liu, Y. Qian, S. Tang, S. Yang, Growth of novel nanostructured copper oxide (CuO) films on copper foil, Journal of Crystal Growth 291 (2006) 479–484.
[3] M.S. Hassan, T. Amna, O.B. Yang, M.H. El-Newehy, S.S. Al-Deyab, M.S. Khil, Smart copper oxide nanocrystals: synthesis, characterization, electrochemical and potent antibacterial activity, Colloids and Surfaces B: Biointerfaces 97 (2012) 201–206.
[4] M. Vaseem, A. Umar, Y.B. Hahn, D.H. Kim, K.S. Lee, J.S. Jang, J.S. Lee, Flower-shaped CuO nanostructures: structural, photocatalytic and XANES studies, Catalysis Communications 10 (2008) 11–16.
[5] Q. Yang, P.X. Yan, J.B. Chang, J.J. Feng, G.H. Yue, Growth of bicrystal CuO microsheets from aqueous solution, Physics Letters A 361 (2007) 493–496.
[6] C.H. Xu, C.H. Woo, S.Q. Shi, Formation of CuO nanowires on Cu foil, Chemical Physics Letters 399 (2004) 62–66.
[7] D. Shang, K. Yu, Y. Zhang, J. Xu, J. Wu, Y. Xu, L. Li, Z. Zhu, Magnetic and field emission properties of straw-like CuO nanostructures, Applied Surface Science 255 (2009) 4093–4096.
[8] Z. Yang, J. Xu, W. Zhang, A. Liu, S. Tang, Controlled synthesis of CuO nanostructures by a simple solution route, Journal of Solid State Chemistry 180 (2007) 1390–1396.
[9] A. Aslani, V. Oroojpour, CO gas sensing of CuO nanostructures, synthesized by an assisted solvothermal wet chemical route, Physica B 406 (2011) 144–149.
[10] J.T. Chen, F. Zhang, J. Wang, G.A. Zhang, B.B. Miao, X.Y. Fan, D. Yan, P.X. Yan, CuO nanowires synthesized by thermal oxidation route, Journal of Alloys and Compounds 454 (2008) 268–273.
[11] X. Tao, L. Sun, Y. Zhao, Sonochemical synthesis and characterization of disk-like copper microcrystals, Materials Chemistry and Physics 125 (2011) 219–223.
[12] S. Anandan, G.J. Lee, J.J. Wu, Sonochemical synthesis of CuO nanostructures with different morphology, Ultrasonics Sonochemistry 19 (2012) 682–686.
[13] H. Wang, J.Z. Xu, J.J. Zhu, H.Y. Chen, Preparation of CuO nanoparticles by microwave irradiation, Journal of Crystal Growth 244 (2002) 88–94.
[14] L. Guo, F. Tong, H. Liu, H. Yang, J. Li, Shape-controlled synthesis of self-assembly cubic CuO nanostructures by microwave, Materials Letters 71 (2012) 32–35.
[15] J. Ramyadevi, K. Jeyasubramanian, A. Marikani, G. Rajakumar, A.A. Rahuman, Synthesis and antimicrobial activity of copper nanoparticles, Materials Letters 71 (2012) 114–116.
[16] L. Zheng, X. Liu, Solution-phase synthesis of CuO hierarchical nanosheets at near-neutral pH and near-room temperature, Materials Letters 61 (2007) 2222–2226.
[17] S. Anandan, X. Wen, S. Yang, Room temperature growth of CuO nanorod arrays on copper and their application as a cathode in dye-sensitized solar cells, Materials Chemistry and Physics 93 (2005) 35–40.
[18] S. Jana, S. Das, N.S. Das, K.K. Chattopadhyay, CuO nanostructures on copper foil by a simple wet chemical route at room temperature, Materials Research Bulletin 45 (2010) 693–698.
[19] A.J. Huh, Y.J. Kwon, "Nanoantibiotics": a new paradigm for treating infectious diseases using nanomaterials in the antibiotics resistant era, Journal of Controlled Release 156 (2011) 128–145.
[20] K.H. Tam, A.B. Djurišić, C.M.N. Chan, Y.Y. Xi, C.W. Tse, Y.H. Leung, W.K. Chan, F.C.C. Leung, D.W.T. Au, Antibacterial activity of ZnO nanorods prepared by a hydrothermal method, Thin Solid Films 516 (2008) 6167–6174.
[21] P. Bhadra, M.K. Mitra, G.C. Das, R. Dey, S. Mukherjee, Interaction of chitosan capped ZnO nanorods with *Escherichia coli*, Materials Science and Engineering C 31 (2011) 929–937.
[22] Powder Diffract. File, JCPDS-ICDD, 12 Campus Boulevard, Newtown Square, PA 19073-3273, U.S.A. 2001.
[23] A. Ahmed, N.S. Gajbhiye, A.G. Joshi, Low cost, surfactant-less, one pot synthesis of Cu_2O nano-octahedra at room temperature, Journal of Solid State Chemistry 184 (2011) 2209–2214.
[24] C. Boudias, D. Monceau, CaRIne Crystallography 3.1, DIVERGENT S. A., Centre de Transfert, 60200 Compiègne, France, 1989–1998.
[25] A.P. Moura, L.S. Cavalcante, J.C. Sczancoski, D.G. Stroppa, E.C. Paris, A.J. Ramirez, J.A. Varela, E. Longo, Structure and growth mechanism of CuO plates obtained by microwave-hydrothermal without surfactants, Advanced Powder Technology 21 (2010) 197–202.
[26] S.S. Chang, H.J. Lee, H.J. Park, Photoluminescence properties of spark-processed CuO, Ceramics International 31 (2005) 411–415.
[27] G. Applerot, N. Perkas, G. Amirian, O. Girshevitz, A. Gedanken, Coating of glass with ZnO via ultrasonic irradiation and a study of its antibacterial properties, Applied Surface Science 256S (2009) S3–S8.
[28] S. Anitha, B. Brabu, D.J. Thiruvadigal, C. Gopalakrishnan, T.S. Natarajan, Optical, bactericidal and water repellent properties of electrospun nano-composite membranes of cellulose acetate and ZnO, Carbohydrate Polymers 87 (2012) 1065–1072.

[29] R. Jalal, E.K. Goharshadi, M. Abareshi, M. Moosavi, A. Yousefi, P. Nancarrow, ZnO nanofluids: green synthesis, characterization, and antibacterial activity, Materials Chemical Physics 121 (2010) 198–201.
[30] Y. Ku, Y.H. Huang, Y.C. Chou, Preparation and characterization of ZnO/TiO_2 for the photocatalytic reduction of Cr(VI) in aqueous solution, Journal of Molecular Catalysis A: Chemical 342–343 (2011) 18–22.
[31] V. Stranak, H. Wulff, H. Rebl, C. Zietz, K. Arndt, R. Bogdanowicz, B. Nebe, R. Bader, A. Podbielski, Z. Hubicka, R. Hippler, Deposition of thin titanium-copper films with antimicrobrial effect by advanced magnetron sputtering methods, Materials Science and Engineering C 31 (2011) 1512–1519.

Hindawi Publishing Corporation
Journal of Nanomaterials
Volume 2013, Article ID 208230, 4 pages
http://dx.doi.org/10.1155/2013/208230

Hindawi

Research Article

Photoluminescence of Hexagonal ZnO Nanorods Hydrothermally Grown on Zn Foils in KOH Solutions with Different Values of Basicity

Nuengruethai Ekthammathat,[1] Titipun Thongtem,[1,2] Anukorn Phuruangrat,[3] and Somchai Thongtem[2,4]

[1] *Department of Chemistry, Faculty of Science, Chiang Mai University, Chiang Mai 50200, Thailand*
[2] *Materials Science Research Center, Faculty of Science, Chiang Mai University, Chiang Mai 50200, Thailand*
[3] *Department of Materials Science and Technology, Faculty of Science, Prince of Songkla University, Hat Yai, Songkhla 90112, Thailand*
[4] *Department of Physics and Materials Science, Faculty of Science, Chiang Mai University, Chiang Mai 50200, Thailand*

Correspondence should be addressed to Titipun Thongtem; ttpthongtem@yahoo.com and Anukorn Phuruangrat; phuruangrat@hotmail.com

Received 18 November 2012; Revised 19 February 2013; Accepted 25 February 2013

Academic Editor: Yun Zhao

Aligned hexagonal ZnO nanorods on pure Zn foils were hydrothermally synthesized in 30 mL solutions containing 0.05–0.50 g KOH. The products were characterized by X-ray diffraction (XRD), scanning electron microscopy (SEM), transmission electron microscopy (TEM), and photoluminescence (PL) spectroscopy. In this research, wurtzite hexagonal ZnO nanorods grown along the [002] direction with green light emission at 541 nm caused by singly ionized oxygen vacancies inside were detected.

1. Introduction

One-dimensional (1D) semiconducting materials are able to be used for a number of potential applications in short wavelength optical, nanoelectronic, and optoelectronic devices due to their tunable electronic and optoelectronic properties controlled by morphologies and dimensions [1–3]. Compared to two-dimensional (2D), three-dimensional (3D), and zero-dimensional (0D) nanostructures, the 1D nanostructure has unique characteristic: large aspect ratio, single crystalline structure, and oriented growth [3]. Zinc oxide is an important low-cost II–VI basic semiconductor with 3.37 eV wide band gap and strong exciton binding energy of 60 meV at room temperature [4–7]. It possesses unique catalytic, electrical, optoelectronic, and photochemical properties—very interesting for a number of potential applications as room-temperature UV lasers, sensors, light-emitting diodes, optical switches, solar cells, and photocatalysis due to its low dielectric constant, high chemical stability, good photoelectric, and piezoelectric behaviors [4, 6, 8].

In the paper, hexagonal ZnO nanorods on Zn foils were hydrothermally synthesized in solutions containing 0.05–0.50 g KOH at 120°C. Their phase, morphology, and photoluminescence were investigated and discussed in more details.

2. Experimental Procedure

Reagents of the research were of analytical grade and used without further purification. The hexagonal prism ZnO nanorods were grown on Zn foils by the following. Several 10 × 10 mm square Zn foils with 0.25 mm thick were cleaned with deionized water and absolute alcohol in an ultrasound bath and put in 30 mL of 0.05, 0.10, 0.20, 0.30, 0.40, and 0.50 g KOH aqueous solutions, containing 1, 2, 4, 6, 8, and 10 times of KOH in sequence. All of the solutions and zinc foils were transferred into 50 mL Teflon-lined stainless steel autoclaves, which were tightly closed, heated at 120°C in a laboratory electric oven for 24 h, and naturally cooled to room temperature. In the end, the zinc foils were thoroughly rinsed by

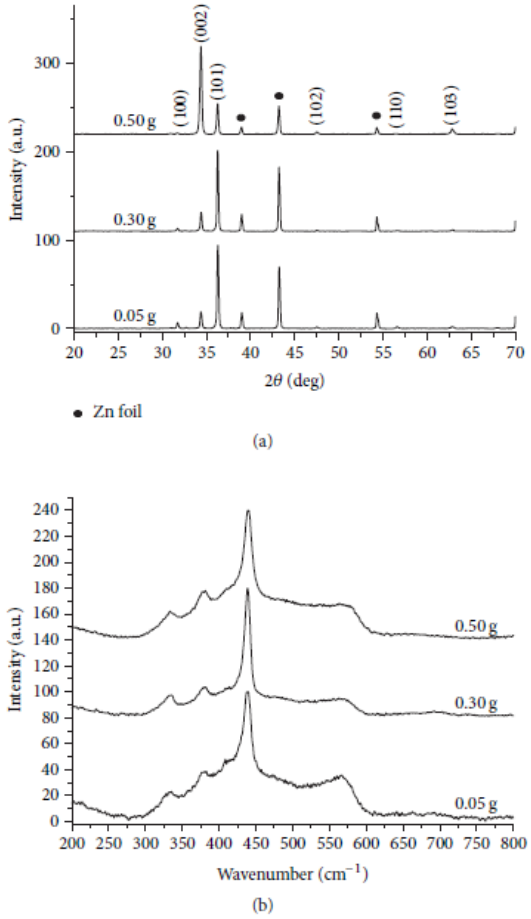

FIGURE 1: (a) XRD patterns and (b) Raman spectra of the as-synthesized ZnO in 30 mL solutions containing 1 (0.05 g), 6 (0.30 g) and 10 times (0.50 g) of KOH.

deionized water several times and alcohol, and dried at 70°C in an electric oven for 12 h for further characterization.

X-ray diffraction (XRD) operated on Philips X'Pert MPD X-ray diffractometer with Cu K_α radiation in the 2θ of 20–70 deg with a scanning rate of 0.02 deg per step and Raman spectroscopy on T64000 HORIBA Jobin Yvon at 50 mW Ar Laser with 514.5 nm wavelength were used to determine phase, crystalline degree, purity, and vibration modes. Their morphologies were characterized by scanning electron microscopy (SEM, JEOL JSM-6335F) with an accelerating voltage of 15 kV across the LaB_6 cathode. Their nanostructures and growth direction were further investigated by transmission electronic microscopy (TEM) and selected area electronic diffraction (SAED) on a JEOL JEM-2010 TEM at 200 kV with LaB_6 gun. At the end, optical properties of the products were analyzed by a LS50B *Perkin Elmer* fluorescence spectrometer in the wavelength range of 450–700 nm.

3. Results and Discussion

Figure 1(a) exhibits typical XRD patterns of the as-grown ZnO on Zn foils, revealing that all diffraction peaks were explicable in term of wurtzite ZnO structure with $a = b = 3.251$ Å and $c = 5.208$ Å (JCPDS No. 36-1451) [9]. Sharp diffraction peaks indicate good crystalline degree of the as-synthesized crystals without other impurities detection.

Degree of c orientation of the as-synthesized ZnO samples was explained by the relative texture coefficient (TC) [10, 11] of the (002) peak calculated using the formula

$$\mathrm{TC}_{002} = \frac{\left(I_{002}/I^0_{002}\right)}{\left[I_{002}/I^0_{002} + I_{100}/I^0_{100}\right]} \quad (1)$$

TC_{002} is the relative texture coefficient of the (002) over (100) diffraction peaks. I_{002} and I_{100} are the measured diffraction intensities of the (002) and (100) peaks, including the corresponding I^0_{002} and I^0_{100} values of the randomly oriented standard powder, respectively. For randomly crystallographic orientation, the texture coefficient of ZnO is 0.5. In the solution containing 0.50 g KOH, calculated TC_{002} was 0.86, which supported the preferential orientation of the as-synthesized ZnO nanorods grown along the [002] direction on the Zn foil.

Wurtzite ZnO structure belongs to C^4_{6v} ($P6_3mc$) space group with two formula units per primitive cell, and all atoms occupy the C^{3v} sites. Group theory of wurtzite ZnO structure predicts eight sets of phonon modes: $A_1 + E_1 + 2E_2$ (Raman active), $2B_2$ (Raman silent), and $A_1 + E_1$ (IR active). Moreover, the A_1 and E_1 symmetry are split into longitudinal (L) and transverse (T) optical (O) components due to the macroscopic electric fields associated with the LO phonons. Figure 1(b) shows Raman spectra of the as-synthesized ZnO nanorods. They show a dominant peak of typical characteristic of the wurtzite ZnO structure at 439 cm^{-1}, assigned to be the optical phonon E_{2H} mode. The weak peak at 332 cm^{-1} was assigned to be the second-order Raman scattering arising from the zone/zero boundary phonons E_{2H}–E_{2L} of multiphonon process, while the Raman peak at 379 cm^{-1} is attributed to A_1 symmetry with the TO mode. Furthermore, Raman spectra of ZnO samples at 567 cm^{-1} are a contribution of the E_1 (LO) mode which is directly associated with oxygen vacancies. The stronger E_1 (LO) mode indicates the presence of higher oxygen vacancies inside [5, 12–14].

SEM images as shown in Figure 2 were investigated on surfaces of Zn foils after hydrothermal treatment in 30 mL solutions containing 1 (0.05 g), 2 (0.10 g), 4 (0.20 g), 6 (0.30 g), 8 (0.40 g), and 10 times (0.50 g) of KOH. An interesting feature of the nanostructures grown on the bottom surfaces exhibited the presence of aligned nanorods of ZnO with the diameter ranging from 400 nm to 700 nm without the detection of other nanostructures. The lengths of the ZnO nanorods are in the range of several micrometers to even longer than 5–7 μm. These nanorods were enlarged and lengthened in sequence with an increase in the degree of basicity. The inset of Figure 2(f) demonstrates the hexagonal

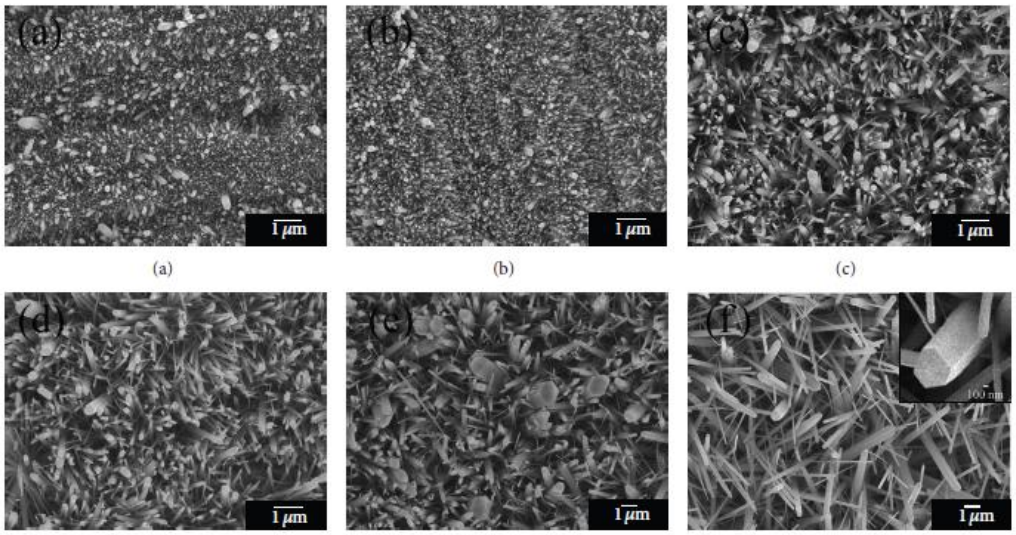

FIGURE 2: SEM images of the as-synthesized ZnO samples in 30 mL solutions containing (a) 1 (0.05 g), (b) 2 (0.10 g), (c) 4 (0.20 g), (d) 6 (0.30 g), (e) 8 (0.40 g), and (f) 10 times (0.50 g) of KOH.

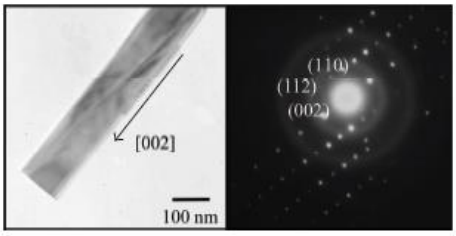

FIGURE 3: TEM image and SAED pattern of hexagonal ZnO nanorod in 30 mL solution containing 10 times (0.50 g) of KOH.

ZnO nanorod which was fully grown on Zn foil in the solution containing 0.50 g KOH.

The hexagonal ZnO nanorods were also characterized through TEM and SAED (Figure 3). TEM image reveals a single hexagonal ZnO nanorod with smooth surface and the preferred growth in the [002] direction. It shows the SAED pattern of bright spots corresponding to hexagonal wurtzite ZnO [9].

Based on the previous discussion, mechanism of the growth and morphology of ZnO nanostructure can be proposed as follows:

$$\mathrm{Zn} + 2\mathrm{H_2O} + 2\mathrm{OH^-} \longrightarrow \mathrm{Zn(OH)_4^{2-}} + \mathrm{H_2} \quad (2)$$

$$\mathrm{Zn(OH)_4^{2-}} \longrightarrow \mathrm{ZnO} + \mathrm{H_2O} + 2\mathrm{OH^-} \quad (3)$$

The formation of $Zn(OH)_4^{2-}$ ions from Zn^{2+} and OH^- ions by a hydrothermal reaction is a key role in the formation of hexagonal wurtzite ZnO nanorods. The primary ZnO nanoparticles began to nucleate on Zn foil by the dissolution of Zn atoms into the solution and the cause of concentration gradient of Zn^{2+}. The intrinsic electric fields of the polar ZnO lattice could be responsible for further growth of ZnO crystals, described as alternating planes of Zn^{2+} and O^{2-}, stacked along the *c*-axis. The oppositely charged ions produced positively charged and negatively charged surfaces, resulting in polarization along the *c*-axis. The preferred *c*-axis orientation of ZnO nanostructure is driven by electrostatic interaction between the polar charges to minimize surface energy. Finally, ZnO nanorods grew on Zn foil as substrate [15].

The main emission of ZnO nanorods can be assigned as the recombination of free excitons. Other peaks probably originated from position of band-edge emission of ZnO of relatively large dimensions with different concentration of native defects [16]. It is well known that visible photoluminescence mainly originates from defect states of Zn interstitials, zinc vacancies, and oxygen vacancies [17]. Photoluminescence (PL) of ZnO nanorods grown on Zn foils was investigated using excitation wavelength of 214 nm at room temperature as shown in Figure 4. PL spectrum of hexagonal ZnO nanorods using 0.50 g KOH shows the highest strong green light emission at 541 nm, due to the singly ionized oxygen vacancies of ZnO, in accordance with other reports [16–18].

4. Conclusions

In summary, densely aligned hexagonal ZnO nanorods on Zn foils were synthesized by a 120°C and 24 h hydrothermal reaction. The XRD, SEM, and TEM analyses showed that the

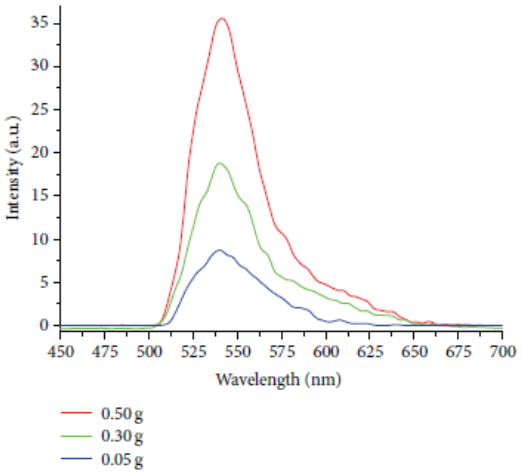

FIGURE 4: PL spectra of the as-synthesized ZnO in 30 mL solutions containing 1 (0.05 g), 6 (0.30 g), and 10 times (0.50 g) of KOH.

as-synthesized products were pure wurtzite ZnO nanorods with uniform hexagonal structure of 400–700 nm diameter and 5–7 μm long. Room temperature PL spectrum of the ZnO nanorods exhibited one strong green light emission at 541 nm due to the singly ionized oxygen vacancies inside.

Acknowledgments

The authors wish to thank the Thailand's Office of the Higher Education Commission for providing financial support through the National Research University (NRU) Project for Chiang Mai University (CMU) and the Human Resource Development Project in Science Achievement Scholarship of Thailand (SAST) and the Thailand Research Fund (TRF) for providing financial support through the TRF Research Grant BRG5380020, including the Graduate School of CMU through a general support.

References

[1] L. Z. Pei, H. S. Zhao, W. Tan, H. Y. Yu, Y. W. Chen, and Q. F. Zhang, "Single crystalline ZnO nanorods grown by a simple hydrothermal process," *Materials Characterization*, vol. 60, no. 9, pp. 1063–1067, 2009.

[2] Z. Li, X. Huang, J. Liu, Y. Li, and G. Li, "Morphology control and transition of ZnO nanorod arrays by a simple hydrothermal method," *Materials Letters*, vol. 62, no. 10-11, pp. 1503–1506, 2008.

[3] X. Wu, H. Chen, L. Gong, F. Qu, and Y. Zheng, "Low temperature growth and properties of ZnO nanorod arrays," *Advances in Natural Sciences*, vol. 2, Article ID 035006, 2011.

[4] H. Zhang, J. Feng, J. Wang, and M. Zhang, "Preparation of ZnO nanorods through wet chemical method," *Materials Letters*, vol. 61, no. 30, pp. 5202–5205, 2007.

[5] J. H. Yang, J. H. Zheng, H. J. Zhai, L. L. Yang, J. H. Lang, and M. Gao, "Growth mechanism and optical properties of ZnO nanosheets by the hydrothermal method on Si substrates," *Journal of Alloys and Compounds*, vol. 481, no. 1-2, pp. 628–631, 2009.

[6] X. Ren, D. Han, D. Chen, and F. Tang, "Large-scale synthesis of hexagonal cone-shaped ZnO nanoparticles with a simple route and their application to photocatalytic degradation," *Materials Research Bulletin*, vol. 42, no. 5, pp. 807–813, 2007.

[7] S. Suwanboon, R. Tanattha, and R. Tanakorn, "Fabrication and properties of nanocrystalline zinc oxide thin film prepared by sol-gel method," *Songklanakarin Journal of Science and Technology*, vol. 30, no. 1, pp. 65–69, 2008.

[8] D. Wang, C. Song, Z. Hu, W. Chen, and X. Fu, "Growth of ZnO prisms on self-source substrate," *Materials Letters*, vol. 61, no. 1, pp. 205–208, 2007.

[9] Powder Diffract, File, JCPDS Internat. Centre Diffract. Data, PA, 19073–3273, U.S.A, 2001.

[10] J. H. Park, P. Muralidharan, and D. K. Kim, "Solvothermally grown ZnO nanorod arrays on (101) and (002) single- and polycrystalline Zn metal substrates," *Materials Letters*, vol. 63, no. 12, pp. 1019–1022, 2009.

[11] F. Li, Z. Li, and F. J. Jin, "Structural and luminescent properties of ZnO nanorods," *Materials Letters*, vol. 61, no. 8-9, pp. 1876–1880, 2007.

[12] L. l. Yang, J. H. Yang, D. D. Wang et al., "Photoluminescence and Raman analysis of ZnO nanowires deposited on Si(100) via vapor-liquid-solid process," *Physica E*, vol. 40, no. 4, pp. 920–923, 2008.

[13] O. Lupan, L. Chow, L. K. Ono et al., "Synthesis and characterization of Ag- or Sb-doped ZnO nanorods by a facile hydrothermal route," *Journal of Physical Chemistry C*, vol. 114, no. 29, pp. 12401–12408, 2010.

[14] S. J. Chen, Y. C. Liu, Y. M. Lu, J. Y. Zhang, D. Z. Shen, and X. W. Fan, "Photoluminescence and Raman behaviors of ZnO nanostructures with different morphologies," *Journal of Crystal Growth*, vol. 289, no. 1, pp. 55–58, 2006.

[15] J. Y. Kim, H. Jeong, and D. J. Jang, "Hydrothermal fabrication of well-ordered ZnO nanowire arrays on Zn foil: room temperature ultraviolet nanolasers," *Journal of Nanoparticles Research*, vol. 13, no. 12, pp. 6699–6706, 2011.

[16] W. Li, Y. Sun, and J. Xu, "Controllable hydrothermal synthesis and properties of ZnO hierarchicalmicro/nanostructures," *Nano-Micro Letters*, vol. 4, no. 2, pp. 98–102, 2012.

[17] Y. J. Gao, W. C. Zhang, X. L. Wu et al., "Hydrothermal self-assembling of ZnO nanorods into sphere-like superstructures and their optical characteristics," *Applied Surface Science*, vol. 255, no. 5, pp. 1982–1987, 2008.

[18] G. Z. Wang, N. G. Ma, C. J. Deng et al., "Large-scale synthesis of aligned hexagonal ZnO nanorods using chemical vapor deposition," *Materials Letters*, vol. 58, no. 16, pp. 2195–2198, 2004.

Powder Technology 254 (2014) 199–205

Contents lists available at ScienceDirect

Powder Technology

journal homepage: www.elsevier.com/locate/powtec

Characterization and antibacterial activity of nanostructured ZnO thin films synthesized through a hydrothermal method

Nuengruethai Ekthammathat [a], Somchai Thongtem [b,c,*], Titipun Thongtem [a,c,**], Anukorn Phuruangrat [d]

[a] Department of Chemistry, Faculty of Science, Chiang Mai University, Chiang Mai 50200, Thailand
[b] Department of Physics and Materials Science, Faculty of Science, Chiang Mai University, Chiang Mai 50200, Thailand
[c] Materials Science Research Center, Faculty of Science, Chiang Mai University, Chiang Mai 50200, Thailand
[d] Department of Materials Science and Technology, Faculty of Science, Prince of Songkla University, Hat Yai, Songkhla 90112, Thailand

ARTICLE INFO

Article history:
Received 3 August 2013
Received in revised form 9 December 2013
Accepted 6 January 2014
Available online 13 January 2014

Keywords:
Nanostructured ZnO
Hydrothermal reaction
Electron microscopy
Antibacterial properties

ABSTRACT

Nanostructured ZnO films have been successfully synthesized on Zn substrates by a simple hydrothermal method at 120 °C in 24 h. The morphologies of the products were controlled by the following alkaline precursor solutions: NaOH, LiOH and NH_4OH, which played a role in the crystallization process by generating rod-like, pencil-like and star-like particles, respectively. The phase and crystallinity of the nanostructured films were characterized by X-ray diffraction and selected area electron diffraction, the vibrational modes were determined by Fourier transform infrared spectrometry and Raman spectroscopy, and their morphologies were visualized by scanning electron microscopy and transmission electron microscopy. The photoluminescence of the products exhibited a strong green–yellow band emission at 540 nm. By using the inhibition zone method, the as-synthesized ZnO nanostructures were observed to inhibit bacterial activity.

1. Introduction

Nanostructured materials have a variety of different properties compared to bulk materials, due to their surface features, quantum size and macroscopic quantum tunneling effects [1,2]. These materials exhibit an interesting size-dependence based on electrical, optical, magnetic and chemical properties that bulk materials are unable to achieve [1,3]. Thus, the synthesis of uniformly sized nanomaterials is of key importance. The physical and chemical properties are strongly dependent on their dimension and are broadly referred to as size effects [3]. The most important requirement in the synthesis of nanomaterials is the ability to control their size and shape, including the maintenance of their uniformity [3,4]. The size of the nanocrystals also significantly influences the electronic diffusion process [4]. The most popular demonstration of the size-dependent characteristics of nanomaterials is a continuous fluorescent emission from semiconducting nanomaterials [5]. Their shapes can play a critical role in determining such properties as the energy gap (E_g) [4]. The shapes of nanomaterials can be simply classified based on their dimensionality [4]: one-dimensional (1D) nanorods and nanowires [4] exhibit superior optical and electrical properties that originate from scaling down their dimensions to the length scale by comparing them to the de Broglie wavelength of the carriers [6].

Among the prominent metal-oxide materials, ZnO has been intensively investigated for potential applications in piezoelectric [7], electronic [7,8], gas sensing [9], photocatalysis [8,9], optoelectronic devices [6–8] and, especially, as materials for room temperature ultraviolet (UV) laser diodes [6] and data storage units [8]. ZnO has the well-known specific electrical and optoelectronic properties of II–VI semiconductors [2,9] with a wide band gap of 3.37 eV and a large exciton binding energy of 60 meV at room temperature [2,8–10] that is greater than its thermal energy at room temperature (26 meV) [6]. In recent years, 1D ZnO nanostructured arrays on a variety of substrates have attracted considerable interest because of their specific optoelectronic and field-emission characteristics originating from their unique heterogeneous crystalline structures, leading to promising applications in the fabrication of functional nano-/micro-devices [11]. Films with well-aligned ZnO nanorods or nanowires may exhibit much larger surface areas than ZnO films synthesized from randomly oriented nanoparticles [11]. Moreover, these nanorods are packed notably densely, enabling the fast and effective diffusion of electrons, and they are used for lasers and solar cells [11]. Recently, ZnO films of nanostructures have been fabricated on a variety of substrates, including Si [6,9], glass [7,10] and indium tin oxide (ITO) [12,13], by several different methods: chemical vapor deposition (CVD) [6], thermal evaporation [6], sol–gel [7], etching [8], hydrothermal [11]/solvothermal routes [14] and electrodeposition [13,15].

In this research, nanostructured ZnO films on Zn substrates were hydrothermally synthesized in solutions containing NaOH, LiOH and

* Correspondence to: S. Thongtem, Department of Physics and Materials Science, Faculty of Science, Chiang Mai University, Chiang Mai 50200, Thailand. Tel.: +66 53 941924; fax: +66 53 943445.
** Correspondence to: T. Thongtem, Department of Chemistry, Faculty of Science, Chiang Mai University, Chiang Mai 50200, Thailand. Tel.: +66 53 943344; fax: +66 53 892277.
E-mail addresses: schthongtem@yahoo.com (S. Thongtem), ttpthongtem@yahoo.com (T. Thongtem).

0032-5910/$ – see front matter © 2014 Elsevier B.V. All rights reserved.
http://dx.doi.org/10.1016/j.powtec.2014.01.010

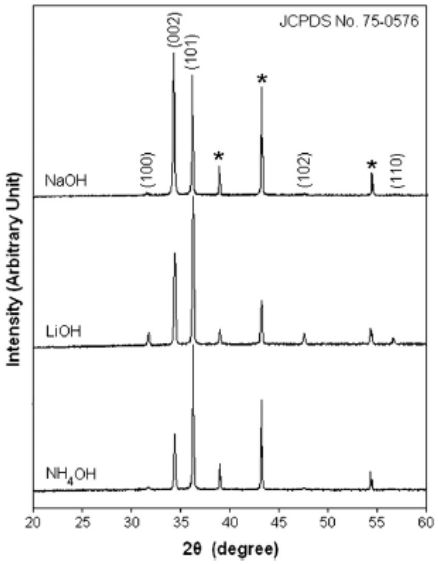

Fig. 1. XRD patterns of ZnO synthesized in NaOH, LiOH and NH_4OH alkaline precursor solutions.

NH_4OH without using any catalysts or templates through a common, simple, safe and low-cost method. The effects of the as-synthesized ZnO with different morphologies were studied and reported with respect to their properties and applications for photoluminescence and antibacterial activity.

2. Experimental methods

Zinc foils (15 mm × 15 mm × 0.25 mm), used as both a solid reagent and as substrates for the direct growth of nanostructured ZnO films, were carefully cleaned in 99% ethanol and DI water containing ultrasound baths. Concurrently, NaOH, LiOH and NH_4OH solutions with the same concentration of 5 M were added to 20 ml DI water to form precursor solutions until the pH values were 12, 12 and 10, respectively. The precursor solutions were put in Teflon-lined stainless steel autoclaves, and the clean Zn foils were added to each solution. The autoclaves were tightly closed, heated at 120 °C for 24 h and left to cool down to room temperature. The as-synthesized films on Zn substrates were rinsed with DI water and ethanol several times and dried at 70 °C for 48 h.

The crystallinity and phases of the products were characterized by an X-ray diffractometer (XRD, Philips X'Pert MPD) using Cu-K_α radiation at 45 kV and 35 mA in the range of 20–60 deg, and the surface morphologies were characterized by both a field emission scanning electron microscope (FE-SEM, JEOL JSM-6335F) operating at 35 kV and a transmission electron microscope (TEM, JEOL JEM-2010) equipped with a selected area electron diffractometer (SAED) operating at 200 kV. The atomic vibrations were measured by a Fourier transform infrared (FTIR, RX Perkin Elmer) spectrometer operating in the range of 400–4000 cm^{-1} at room temperature with ZnO tablets diluted 40-fold with KBr and by a Raman spectrometer (T64000 HORIBA Jobin Yvon) using 50 mW and a 514.5 nm wavelength Ar green laser. The emission wavelength was measured by a photoluminescence (PL, LS 50B Perkin Elmer) spectrometer using a 215 nm excitation wavelength at room temperature, including the investigation of antibacterial activities by different film morphologies.

In this research, two types of bacteria–gram-positive (*Staphylococcus aureus*) and gram-negative (*Escherichia coli*)–were used to study the antibacterial activity of ZnO thin films by the inhibition zone method. Both strains were transferred into flasks containing nutrient broth (NB) with an initial optical density (OD) of 0.1 at a 660 nm orange wavelength; and the bacteria were cultured at 37 °C under aerated conditions until reaching an OD of 0.3. Agar was then added to the flasks. Modified agar diffusion assays (testing disks) were used to determine the antibacterial activity of the ZnO thin films after 24 h incubation at 37 °C by observing the formation of clear zones around the foils.

3. Results and discussion

3.1. XRD

The XRD patterns (Fig. 1) of the ZnO films synthesized in NaOH, LiOH and NH_4OH solutions on Zn substrates were very sharp, indicating the existence of products with good crystalline structure. All diffraction patterns can be indexed to possess a hexagonal wurtzite structure, compared to JCPDS No. 75-0576 [16], including additional peaks marked with asterisks indexed to be Zn substrates compared to JCPDS No. 04-0831 [16]. No characteristic peaks of other impurities were

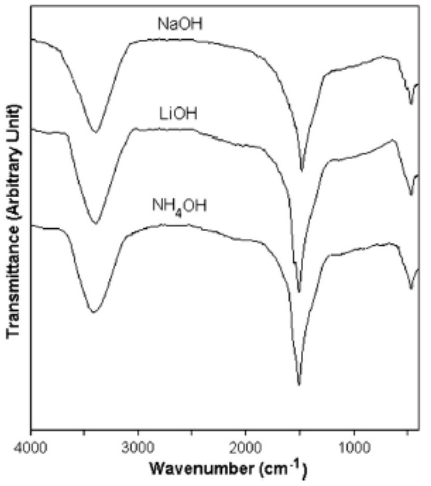

Fig. 2. FTIR spectra of ZnO synthesized in NaOH, LiOH and NH_4OH alkaline precursor solutions.

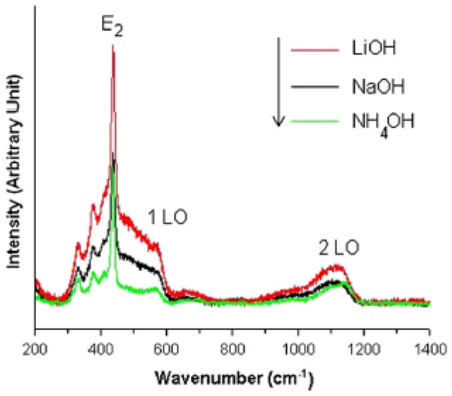

Fig. 3. Raman spectra of ZnO synthesized in NaOH, LiOH and NH_4OH alkaline precursor solutions.

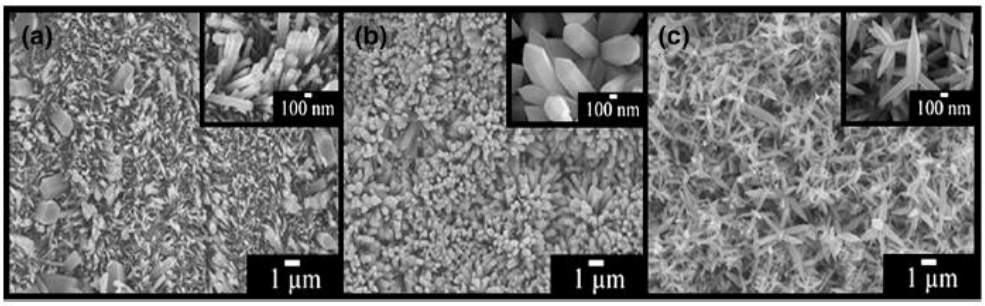

Fig. 4. SEM images of ZnO synthesized in (a) NaOH, (b) LiOH and (c) NH_4OH alkaline precursor solutions.

detected. The XRD pattern of the ZnO product synthesized in NaOH solution showed the highest diffraction peak at 34.45°, which illustrates the texture effect of the highly preferential orientation of the ZnO product along the c-axis perpendicular to the substrate [17]. For product synthesis in the LiOH and NH_4OH solutions, the (101) peaks were at their highest. It should be noted that strong diffraction peaks with the highest relative intensities diffracted from the (002) and (101) planes of the wurtzite hexagonal ZnO phase, suggesting that the 1D ZnO would have preferential growth along the (002) and (101) directions [18], respectively.

3.2. FTIR

FTIR spectroscopy was used to analyze the functional or compositional quality of the products. Fig. 2 shows the FTIR spectra of ZnO synthesized in the solutions containing NaOH, LiOH and NH_4OH over the range of 400–4000 cm^{-1}. Generally, the characteristic peaks of ZnO show bands at 450–600 cm^{-1} [2]. The bands at 480 cm^{-1} are related to the Zn–O stretching vibrations of the tetrahedral surroundings of the Zn atoms [19–21]. The bands at 3490 cm^{-1} correspond to the vibrational modes of the O–H groups, indicating the presence of trace amounts of water adsorbed on the ZnO structured products [2,20,21]. The bands at 1630 cm^{-1} are due to the O–H bending of the water [20].

3.3. Raman analysis

The vibrational properties of as-grown hexagonal structured ZnO were investigated by Raman spectroscopy. In this research, ZnO was in the wurtzite hexagonal phase belonging to the space group C_{6v}^4, having two formula units per primitive cell and all atoms occupying the sites of symmetry C_{3v}. According to group theory, single crystalline ZnO has eight sets of optical phonon modes at the Γ point of the Brillouin zone ($2A_1 + 2B_1 + 2E_1 + 2E_2$). Among these optical phonon modes, the A_1 and E_1 modes are polar in nature and therefore split into two—the transverse optical (TO) and longitudinal optical (LO) phonons. The remaining six optical modes, $A_1 + 2B_1 + E_1 + 2E_2$, can be detected

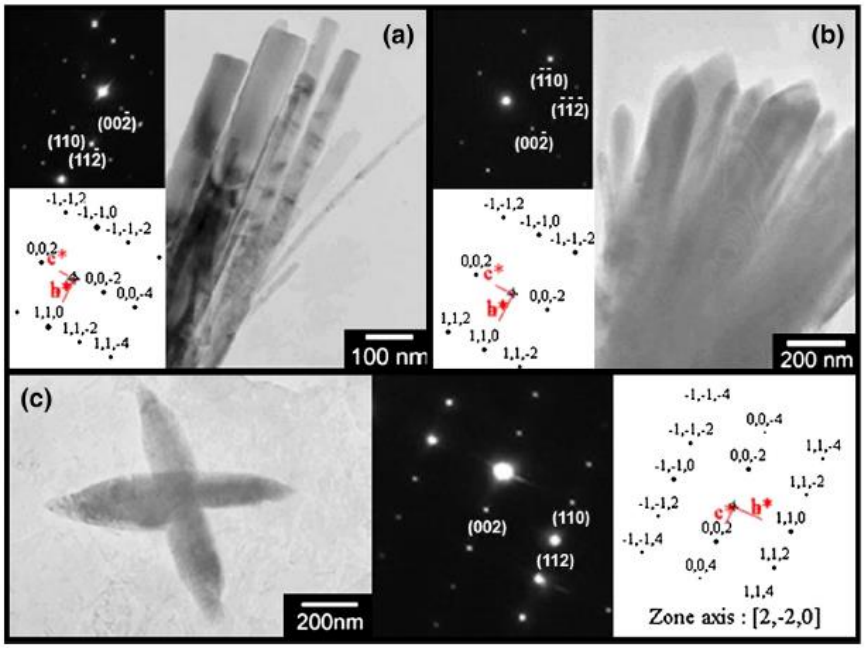

Fig. 5. TEM images, SAED patterns and simulated patterns of ZnO synthesized in (a) NaOH, (b) LiOH and (c) NH_4OH alkaline precursor solutions.

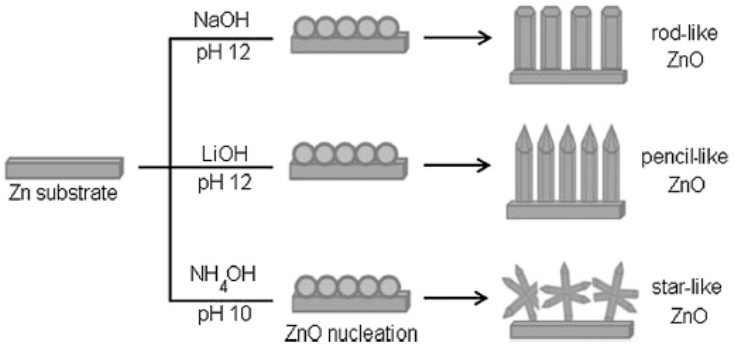

Fig. 6. A schematic diagram for the formation mechanisms of rod-like, pencil-like and star-like ZnO products.

by first-order Raman scattering. The A_1 and E_1 modes are both Raman and infrared (IR) active, but the two E_2 modes are only Raman active. The two B_1 modes are neither Raman nor IR active (silent) modes [22]. Fig. 3 shows the Raman spectra of the as-grown hexagonal structured ZnO on Zn substrates synthesized in NaOH, LiOH and NH_4OH alkaline solutions. The strong peaks at 437 cm^{-1} are due to the Raman active E_2 optical phonon mode (LO) of the ZnO products, confirming that they possess a wurtzite hexagonal crystal structure—in accordance with the above XRD analysis [22,23]. The peaks at 581 cm^{-1} assigned to the A_1 (LO) mode were also detected. These peaks could also be due to the misalignment of rods or the formation of defects, such as zinc interstitials and oxygen vacancies [22]. The second-order vibrational modes were detected at 1110 cm^{-1} [23].

3.4. SEM, TEM and SAED

The low magnification SEM images and their inserts as high magnification images (Fig. 4) show the different morphologies of the ZnO films synthesized on Zn substrates in NaOH, LiOH and NH_4OH alkaline solutions. In this research, ZnO nanorods with an average size of 100 nm in diameter and 500 nm in length, pencil-like ZnO with an approximate size of 300 nm diameter and >800 nm long and 3D star-like ZnO with the average size of each pod being 200 nm in diameter and 1 μm in length were synthesized in NaOH, LiOH and NH_4OH alkaline solutions, respectively.

The phase and morphology of the ZnO products (Fig. 5) were further characterized using TEM and SAED. The TEM images show that the rod-like, pencil-like and star-like ZnO particles were synthesized in solutions containing NaOH, LiOH and NH_4OH, respectively, as the OH^- source—in accordance with the results characterized by SEM. Their corresponding SAED and simulation patterns show spot patterns that were specified as nanostructures of a pure-phase, hexagonal wurtzite-structured ZnO single crystal, which is in good accordance with the above XRD analysis for the phase. These patterns can be identified as the [2–20] zone axis projection of an electron beam on the rod-like, pencil-like and star-like ZnO. The corresponding simulated patterns [24] with lattice vectors (a*, b* and c*) in the (100), (010) and (001) directions are in systematic arrays and are in good accordance with the results obtained by the interpretation.

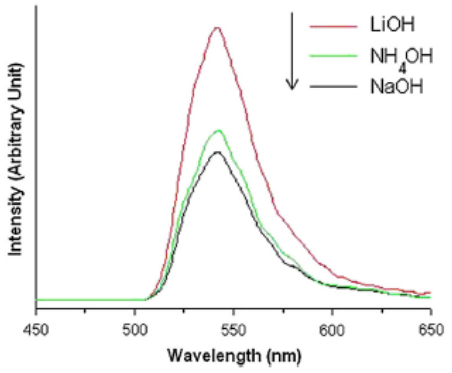

Fig. 7. PL spectra of ZnO synthesized in NaOH, LiOH and NH_4OH alkaline precursor solutions.

3.5. Proposed mechanism

In this research, the synthesis of ZnO nanostructures followed the nucleation and growth stages. Oxygen in the air and in solution has the ability to oxidize the zinc substrate to Zn^{2+} [11]. In the NaOH and LiOH alkaline solutions, $Zn(OH)_4^{2-}$ formed [25]. However, in the NH_4OH alkaline solution, additional $Zn(NH_3)_4^{2+}$ complex ions formed. $Zn(OH)_4^{2-}$ is more stable than $Zn(NH_3)_4^{2+}$, and it is formed by the oxidation of $Zn(NH_3)_4^{2+}$ [11]. During the 120 °C and 24 h hydrothermal reaction in alkaline solutions, $Zn(OH)_4^{2-}$ was present in the solutions as ions. Upon cooling the system down to room temperature, nuclei formed and grew on zinc substrates with different morphologies controlled by Na^+, Li^+ and $(NH_4)^+$ cations contained in the solutions. Finally, the solids were transformed into ZnO by drying at 70 °C. ZnO could also be synthesized by dehydration of the $Zn(OH)_4^{2-}$ ions [26] remaining in the solids.

$$Zn^{2+} + 4OH^- \rightarrow Zn(OH)_4^{2-} \quad (1)$$

$$Zn^{2+} + 4NH_3 \rightarrow [Zn(NH_3)_4]^{2+} \quad (2)$$

$$Zn(NH_3)_4^{2+} + 4OH^- \rightarrow Zn(OH)_4^{2-} + 4NH_3 \quad (3)$$

$$Zn(OH)_4^{2-} \rightarrow ZnO + H_2O + 2OH^- \quad (4)$$

The various morphologies of ZnO were synthesized using the alkaline solution effect. It is a well-known fact that different alkaline solutions play a different role in directing the reaction and crystallization of nanostructures. During hydrothermal processing, a variety of alkali dramatically influenced the precipitation, crystallization, crystal growth and morphology formation [27]. Additionally, the enclosed faces of a crystal are usually those with the slowest growth rate (i.e., the highest surface energy). The surface energy is strongly affected by foreign ions that are adsorbed on the crystal surfaces [28]. The different cations of the various alkaline solutions have an influence on the morphology of

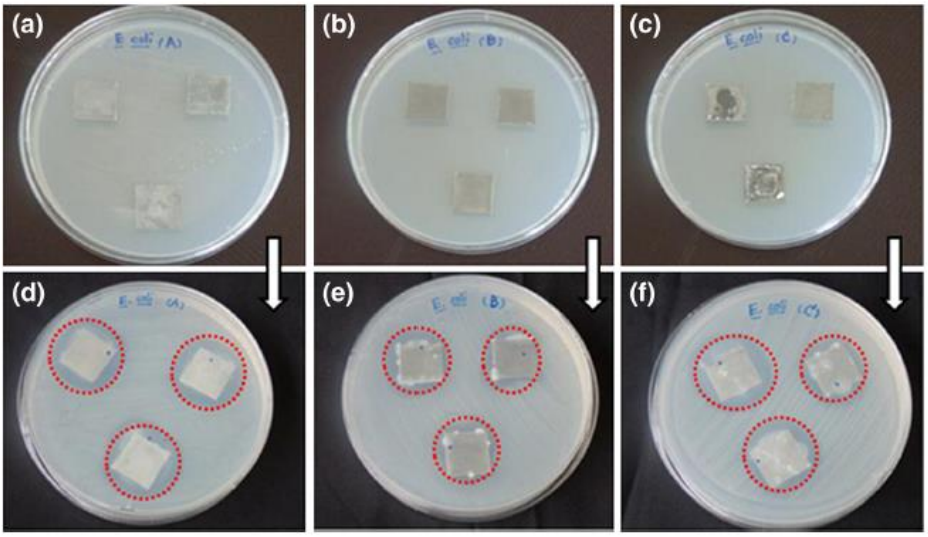

Fig. 8. Effect of *E. coli* inactivation by ZnO synthesized in different alkaline precursor solutions: (a, d) LiOH, (b, e) NaOH and (c, f) NH_4OH; (a–c) before and (d–f) after incubation.

the ZnO products, which developed from nanoparticles into different nanostructures (rod-like, pencil-like and star-like). Wurtzite ZnO with polar structure is hexagonal close packing of oxygen and zinc atoms in 3 m point group and P63mc space group with zinc atoms in tetrahedral sites. The crystalline characteristic of hexagonal wurtzite ZnO with C_{6v} symmetry is well-defined crystallographic (0001) and nonpolar low symmetry (10–10) planes. In case of wurtzite ZnO polar crystal, each Zn^{2+} lies within a tetrahedron of four oxygen atoms. Zinc and oxygen atoms are alternatively arranged along the c-axis such that the Zn-terminated (0001) planes are on top and the O-terminated (000–1) planes are at the bottom. Inherent asymmetry along the c-axis leads to the anisotropic growth of 1D ZnO crystalline solid. The formation of rod-like structured ZnO is believed to be the different growth rates of different crystallographic planes. The hydrothermal growth rate o different planes is as follows: (0001) > (10–1–1) > (10–10). The faste the planes grow, the more rapid they terminate. The relative growth rate of these crystallographic planes determines the aspect ratio and final shape of ZnO products. The (0001) planes terminated due to thei most rapid growth rate leading to the formation of sharp tips at the end of the c axis (pencil-like ZnO). Growth rate of the (10–10) plane was the slowest, thus ZnO solid appeared as nanorods with flat tips (rod-like ZnO). Possibly, Zn atoms on the (0001) metastable polar planes reacted with OH^- ions to form hydroxide species [29,30]. In case of star-like ZnO, the product was composed of symmetric nanorods with sharp tips radially radiating out of the same central core. More active sites originated and more rods grew out of core [26]. In addition, Na^+, Li^+

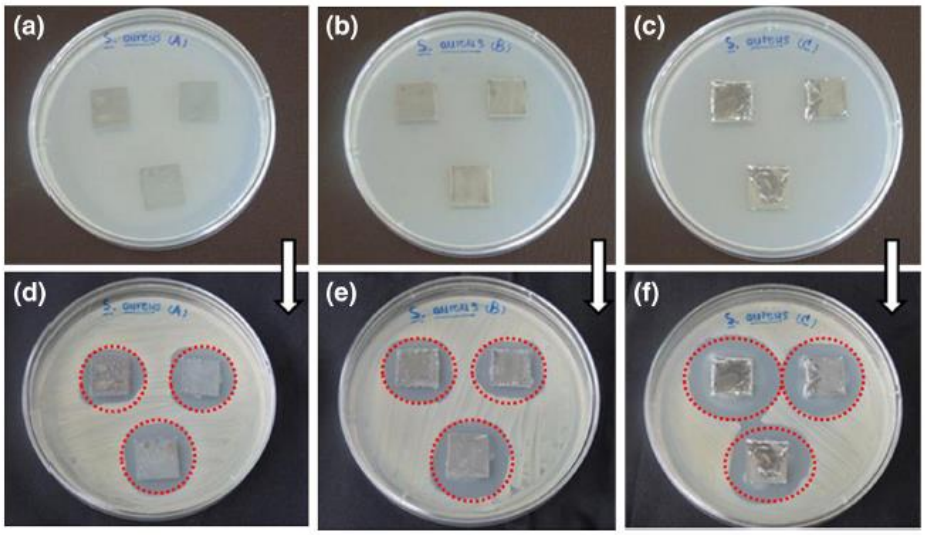

Fig. 9. Effect of *S. aureus* inactivation by ZnO synthesized in different alkaline precursor solutions: (a, d) LiOH, (b, e) NaOH and (c, f) NH_4OH; (a–c) before and (d–f) after incubation.

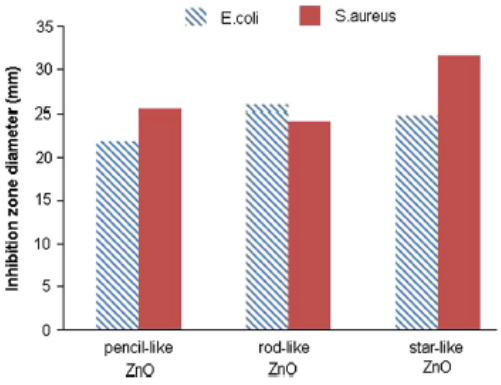

Fig. 10. Comparative analysis of the zone diameter of ZnO with different morphologies on *E. coli* and *S. aureus*.

and $(NH_4)^+$ cations with different masses had different physical properties to attach on the negatively charged O-(000-1) polar surfaces of ZnO crystals. Synthetic path ways of ZnO in the solutions of NaOH and LiOH are different from that of ZnO in the solution of NH_4OH, as the above explanation. These lead to the change in surface energy, growth rate and morphology of ZnO solid. A schematic diagram of the proposed formation mechanism of ZnO nanostructures is shown in Fig. 6.

3.6. PL emission

The room-temperature PL spectra (Fig. 7) of the three ZnO nanostructured films were determined using an excitation wavelength of 215 nm. The green–yellow emission at 540 nm can be detected for all of the products, in accordance with those previously reported [11,20,26]. It should be noted that these nanostructured ZnO emitted photon at the same wavelength but difference in intensity. The emission band was attributed to the radiative recombination of photogenerated holes with the electrons belonging to singly ionized vacancies on the surfaces and subsurfaces [20]. These results suggest that the emission originates from a deep level (DL) defect emission associated with the oxygen vacancies of the ZnO lattices [11,26] related to those of the defects [11].

3.7. Antibacterial activity

The application of the as-synthesized nanostructured ZnO films was investigated in terms of qualitative antibacterial activity by applying the Kirbey–Bauer method [31]. The bactericidal activity was determined based on an inhibition zone. The photographs of Figs. 8 and 9 show the bactericidal activity of *Escherichia coli* and *Staphylococcus aureus*, respectively. Clearly, ZnO could be used as an antibacterial agent for both gram-negative (*Escherichia coli*) and gram-positive (*Staphylococcus aureus*) bacteria. ZnO products with different nanostructures have different physical and chemical properties that promote bactericidal effects (Fig. 10). Zn ions were assumed to have a minor influence on antibacterial activity. The major product responsible for the bactericidal effect was ZnO [32]. The antibacterial activity of ZnO appears to model the role of reactive oxygen species (ROS) generated on the surfaces [31], such as the generation of hydrogen peroxide (H_2O_2) [33,34]. ZnO with defects could be activated by both UV and visible light to create electron–hole (e^-–h^+) pairs, the holes split the H_2O molecules on the ZnO particles into $OH^\bullet$ and H^+. The electrons reacted with oxygen molecules and further reacted with hydrogen ions to produce molecules of H_2O_2 [33,34]. The mechanism of the light-induced generation of ROS could be given as follows [34].

$$ZnO + h\nu \rightarrow ZnO + e^- + h^+ \quad (5)$$

$$h^+ + H_2O \rightarrow OH^\bullet + H^+ \quad (6)$$

$$e^- + O_2 \rightarrow {}^\bullet O_2^- \quad (7)$$

$${}^\bullet O_2^- + H^+ \rightarrow HO_2^\bullet \quad (8)$$

$$HO_2^\bullet + e^- + H^+ \rightarrow H_2O_2 \quad (9)$$

When the interaction was not succeeded, electron–hole pairs would recombine together to generate heat inside ZnO thin films. The generated ROS such as ${}^\bullet O_2^-$, $HO_2^\bullet$, $OH^\bullet$ and H_2O_2 interacted with outer cell walls and further generated free radicals. The radicals penetrated the inner cell membranes and created serious disruption of their internal contents. Thus the cells were deformed, disorganized and leaked [35]. The generated H_2O_2 could penetrate the cell membrane and cause harm to the bacteria [33]. The hydroxyl radicals and superoxide radicals with negatively charged particles could not penetrate the cell membrane and remained in contact with the outer surfaces of the bacteria. Due to the concentration difference, the diffusion process proceeded. The cell walls were cleaved and became elongated, which hindered bacterial activity. A schematic diagram of the antibacterial mechanism (Fig. 11) [31,34,36] is also shown. For these nanostructured ZnO products with different morphologies (rod-like, pencil-like and star-like), there were some differences in emission intensity, photo-generated e^-–h^+ pairs and concentration of the generated ROS, which caused different extent in making harm to bacteria.

4. Conclusions

ZnO nanostructures have been successfully synthesized on Zn substrates through a simple hydrothermal method at 120 °C for 24 h. The morphologies of the hexagonal wurtzite structure were controlled by utilizing different alkaline precursors, which dramatically influenced crystallization progress, precipitation, recrystallization, crystal growth

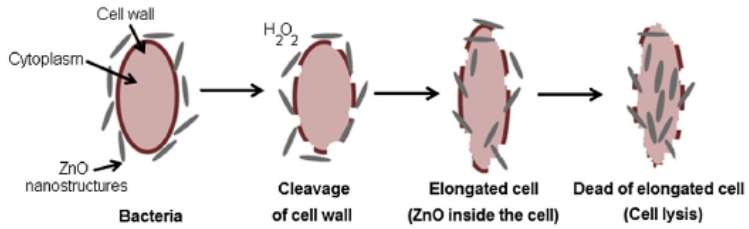

Fig. 11. A schematic diagram of the antibacterial mechanism.

and morphology formation. The as-synthesized products, which were shaped as rods, pencils and stars, were obtained in solutions containing NaOH, LiOH and NH_4OH, respectively. These products emit a green–yellow band at 540 nm, and they exhibit antibacterial activity.

Acknowledgments

We wish to thank the Thailand Office of the Higher Education Commission for providing financial support through the National Research University (NRU) Project for Chiang Mai University and the Human Resource Development Project in Science Achievement Scholarship of Thailand (SAST). We also acknowledge the National Nanotechnology Center (NANOTEC) and the National Science and Technology Development Agency for providing financial support through the project P-10-11345, and we thank the Graduate School of Chiang Mai University for a general support.

References

[1] Y.S. Zhao, H. Fu, A. Peng, Y. Ma, D. Xiao, J. Yao, Low-dimensional nanomaterials based on small organic molecules: preparation and optoelectronic properties, Adv. Mater. 20 (2008) 2859–2876.
[2] Y. Lai, M. Meng, Y. Yu, X. Wang, T. Ding, Photoluminescence and photocatalysis of the flower-like nano-ZnO photocatalysts prepared by a facile hydrothermal method with or without ultrasonic assistance, Appl. Catal. B Environ. 105 (2011) 335–345.
[3] S.G. Kwon, T. Hyeon, Colloidal chemical synthesis and formation kinetics of uniformly sized nanocrystals of metals, oxides, and chalcogenides, Acc. Chem. Res. 41 (2008) 1696–1709.
[4] Y.W. Jun, J.S. Choi, J. Cheon, Shape control of semiconductor and metal oxide nanocrystals through nonhydrolytic colloidal routes, Angew. Chem. Int. Ed. 45 (2006) 3414–3439.
[5] J. Park, J. Joo, S.G. Kwon, Y. Jang, T. Hyeon, Synthesis of monodisperse spherical nanocrystals, Angew. Chem. Int. Ed. 46 (2007) 4630–4660.
[6] W. Lee, M.C. Jeong, J.M. Myoung, Catalyst-free growth of ZnO nanowires by metal-organic chemical vapour deposition (MOCVD) and thermal evaporation, Acta Mater. 52 (2004) 3949–3957.
[7] K.J. Chen, F.Y. Hung, S.J. Chang, S.J. Young, Z.S. Hu, Effects of crystallization on the optical properties of ZnO nano-pillar thin films by sol-gel method, Curr. Appl. Phys. 11 (2011) 1243–1248.
[8] W.K. Tan, K.A. Razak, K. Ibrahim, Z. Lockman, Oxidation of etched Zn foil for the formation of ZnO nanostructure, J. Alloys Compd. 509 (2011) 6806–6811.
[9] C. Liu, Y. Masuda, Y. Wu, O. Takai, A simple route for growing thin films of uniform ZnO nanorod arrays on functionalized Si surfaces, Thin Solid Films 503 (2006) 110–114.
[10] S. Ozturk, N. Kilinc, N. Tasaltin, Z.Z. Ozturk, Fabrication of ZnO nanowires and nanorods, Physica E. 44 (2012) 1062–1065.
[11] Z. Yang, C. Luan, W. Zhang, A. Liu, S. Tang, Fabrication and optical properties of ZnO nanostructured thin films via mechanical oscillation and hydrothermal method, Thin Solid Films 516 (2008) 5974–5980.
[12] K. Yu, Z. Jin, X. Liu, J. Zhao, J. Feng, Shape alterations of ZnO nanocrystal arrays fabricated from $NH_3 \cdot H2O$ solutions, Appl. Surf. Sci. 253 (2007) 4072–4078.
[13] Z. Liu, E. Lei, J. Ya, Y. Xin, Growth of ZnO nanorods by aqueous solution method with electrodeposited ZnO seed layers, Appl. Surf. Sci. 255 (2009) 6415–6420.
[14] J.H. Park, P. Muralidharan, D.K. Kim, Solvothermally grown ZnO nanorod arrays on (101) and (002) single- and polycrystalline Zn metal substrates, Mater. Lett. 63 (2009) 1019–1022.
[15] F.J. Sheini, D.S. Joag, M.A. More, Electrochemical synthesis of Sn doped ZnO nanowires on zinc foil and their field emission studies, Thin Solid Films 519 (2010) 184–189.
[16] Powder Diffract. File, JCPDS Internat. Centre Diffract. Data, PA 19073–3273, U.S.A, 2001.
[17] Z. Li, X. Huang, J. Liu, Y. Li, G. Li, Morphology control and transition of ZnO nanorod arrays by a simple hydrothermal method, Mater. Lett. 62 (2008) 1503–1506.
[18] L.Z. Pei, H.S. Zhao, W. Tan, H.Y. Yu, Y.W. Chen, C.G. Fan, Q.F. Zhang, Hydrothermal oxidization preparation of ZnO nanorods on zinc substrate, Physica E. 42 (2010) 1333–1337.
[19] S.K. Nandi, S. Chakraborty, M.K. Bera, C.K. Maiti, Structural and optical properties of ZnO films grown on silicon and their applications in MOS devices in conjunction with ZrO_2 as a gate dielectric, Bull. Mater. Sci. 30 (2007) 247–254.
[20] N.F. Hamedani, F. Farzaneh, Synthesis of ZnO nanocrystals with hexagonal (wurtzite) structure in water using microwave irradiation, J. Sci. Islam. Repub. Iran 17 (2006) 231–234.
[21] R. Wahab, I.H. Hwang, Y.S. Kim, H.S. Shin, Photocatalytic activity of zinc oxide micro-flowers synthesized via solution method, Chem. Eng. J. 168 (2011) 359–366.
[22] P.S. Kumar, P. Paik, A.D. Raj, D. Mangalaraj, D. Nataraj, A. Gedanken, S. Ramakrishna, Biodegradability study and pH influence on growth and orientation of ZnO nanorods via aqueous solution process, Appl. Surf. Sci. 258 (2012) 6765–6771.
[23] J.T. Chen, J. Wang, R.F. Zhuo, D. Yan, J.J. Feng, F. Zhang, P.X. Yan, The effect of Al doping on the morphology and optical property of ZnO nanostructures prepared by hydrothermal process, Appl. Surf. Sci. 255 (2009) 3959–3964.
[24] C. Boudias, D. Monceau, CaRIne Crystallography 3.1, Centre de Transfert, 60200, DIVERGENT S.A., Compiegne, France, 1989–1998.
[25] Q.R. Hu, S.L. Wang, W.H. Tang, Effects of alkali on the morphologies and photoluminescence properties of ZnO nanostructures, Mater. Lett. 64 (2010) 1822–1824.
[26] H. Zhang, J. Feng, J. Wang, M. Zhang, Preparation of ZnO nanorods through wet chemical method, Mater. Lett. 61 (2007) 5202–5205.
[27] Z. Zhang, J. Mu, Effect of hydrothermal time, pH, and alkali on crystal phase and morphology of manganese oxides, J. Dispers. Sci. Technol. 28 (2007) 793–796.
[28] A. Birkel, N. Loges, E. Mugnaioli, R. Branscheid, D. Koll, S. Frank, M. Panthofer, W. Tremel, Interaction of alkaline metal cations with oxidic surfaces: effect on the morphology of SnO_2 nanoparticles, Langmuir 26 (2010) 3590–3595.
[29] J.H. Yang, J.H. Zheng, H.J. Zhai, L.L. Yang, L. Liu, M. Gao, Solvothermal growth of highly oriented wurtzite-structured ZnO nanotube arrays on zinc foil, Cryst. Res. Technol. 44 (2009) 619–623.
[30] D. Wang, C. Song, Controllable synthesis of ZnO nanorod and prism arrays in a large area, J. Phys. Chem. B 109 (2005) 12697–12700.
[31] J.S. Tawale, K.K. Dey, R. Pasricha, K.N. Sood, A.K. Srivastava, Synthesis and characterization of ZnO tetrapods for optical and antibacterial applications, Thin Solid Films 519 (2010) 1244–1247.
[32] I. Perelshtein, G. Applerot, N. Perkas, E. Wehrschetz-Sigl, A. Hasmann, G.M. Guebitz, A. Gedanken, Antibacterial properties of an in situ generated and simultaneously deposited nanocrystalline ZnO on fabrics, Appl. Mater. Interfaces 1 (2009) 361–366.
[33] M. Eskandari, N. Haghighi, V. Ahmadi, F. Haghighi, S.H.R. Mohammadi, Growth and investigation of antifungal properties of ZnO nanorod arrays on the glass, Physica B 406 (2011) 112–114.
[34] R.K. Dutta, B.P. Nenavathu, M.K. Gangishetty, A.V.R. Reddy, Studies on antibacterial activity of ZnO nanoparticles by ROS induced lipid peroxidation, Colloids Surf. B: Biointerfaces 94 (2012) 143–150.
[35] M.S. Hassan, T. Amna, O.B. Yang, M.H. El-Newehy, S.S. Al-Deyab, M.S. Khil, Smart copper oxide nanocrystals: synthesis, characterization, electrochemical and potent antibacterial activity, Colloids Surf. B: Biointerfaces 97 (2012) 201–206.
[36] R. Wahab, A. Mishra, S.I. Yun, I.H. Hwang, J. Mussarat, A.A. Al-Khedhairy, Y.S. Kim, H.S. Shin, Fabrication, growth mechanism and antibacterial activity of ZnO micro-spheres prepared via solution process, Biomass Bioenergy 39 (2012) 227–239.

CURRICULUM VITAE

Author's Name Ms. Nuengruethai Ekthammathat

Date of Birth 15 November 1986

Place of Birth Chiang Mai, Thailand

Education
2009 Bachelor of Science, Chemistry, Chiang Mai University
2010 Master of Science, Chemistry, Chiang Mai University

Scholarship
2009 -2010, The Center of Excellence for Innovation in Chemistry (PERCH-CIC)
2011 - 2013 The Science achievement of Thailand (SAST)

Publications

1. Anukorn Phuruangrat, Nuengruethai Ekthammathat, Titipun Thongtem, and Somchai Thongtem, "Microwave-assisted synthesis and optical property of $CdMoO_4$ nanoparticles", Journal of Physics and Chemistry of Solids, Vol. 72, 2011, 176-180.
2. Nuengruethai Ekthammathat, Titipun Thongtem, Anukorn Phuruangrat and Somchai Thongtem, "Microwave-assisted synthesis of $CePO_4$ nanorod phosphor with violet emission", Rare Metals, Vol. 30, 2011, 572-576.
3. Anukorn Phuruangrat, Nuengruethai Ekthammathat, T,itipun Thongtem, and Somchai Thongtem, "Glycolthermal synthesis and characterization of hexagonal CdS round microparticles in flower-like clusters", Journal of Alloys and Compounds, Vol. 509, 2011, 10150-10154.
4. Nuengruethai Ekthammathat, Titipun Thongtem, Anukorn Phuruangrat and Somchai Thongtem, "Microwave-assisted synthesis and characterisation of uniform $LaPO_4$ nanorods", Journal of Experimental Nanoscience, Vol. 7, 2012, 616-623.

5. Anukorn Phuruangrat, Nuengruethai Ekthammathat, Somchai Thongtem, and Titipun Thongtem, “Preparation of $LaPO_4$ nanowires with high aspect ratio by a facile hydrothermal method and their photoluminescence”, Research on Chemical Intermediates, Vol. 39, 2012, 1363-1371.
6. Nuengruethai Ekthammathat, Titipun Thongtem, Anukorn Phuruangrat and Somchai Thongtem, “Facile Hydrothermal Synthesis and Optical Properties of Monoclinic CePO4 Nanowires with High Aspect Ratio”, Journal of Nanomaterials, Vol. 2012, ID 958593, 2012, 1-6.
7. Nuengruethai Ekthammathat, Titipun Thongtem, Anukorn Phuruangrat and Somchai Thongtem, “Growth of hexagonal prism ZnO nanorods on Zn substrates by hydrothermal method and their photoluminescence”, Ceramic International, Vol. 39, 2013, S501-S505.
8. Nuengruethai Ekthammathat, Titipun Thongtem, Anukorn Phuruangrat and Somchai Thongtem, “Characterization of ZnO flowers of hexagonal prisms with planar and hexagonal pyramid tips grown on Zn substrates by a hydrothermal process”, Superlattices and Microstructures, Vol. 53, 2013, 195-203.
9. Nuengruethai Ekthammathat, Titipun Thongtem, Anukorn Phuruangrat and Somchai Thongtem, “Photoluminescence of hexagonal ZnO nanorods hydrothermally grown on Zn foils in KOH solutions with different values of basicity”, Journal of Nanomaterials, Vol. 2013, ID 208230, 2013, 1-4.
10. Nuengruethai Ekthammathat, Titipun Thongtem, Anukorn Phuruangrat and Somchai Thongtem, “Synthesis and characterization of $CeVO_4$ by microwave radiation method and its photocatalytic activity”, Journal of Nanomaterials, Vol. 2013, ID 434197, 2013, 1-7.
11. Nuengruethai Ekthammathat, Titipun Thongtem and Somchai Thongtem, “Antimicrobial activities of CuO films deposited on Cu foils by solution chemistry”, Applied Surface Science, Vol. 277 (2013) 211-217.
12. Anukorn Phuruangrat, Pimchanok Jitrou, Phattharanit Dumrongrojthanath, Nuengruethai Ekthammathat, Budsabong Kuntalue, Somchai Thongtem and Titipun Thongtem, “Hydrothermal synthesis and characterization of

$Bi2MoO_6$ nanoplates and their photocatalytic activities", Journal of Nanomaterials, Vol. 2013, ID 789705, 2013, 1-8.

13. Nuengruethai Ekthammathat, Somchai Thongtem, Titipun Thongtem and Anukorn Phuruangrat, "Characterization and antibacterial activity of nanostructured ZnO thin films synthesized through a hydrothermal method", Powder Technology, Vol. 254, 2014, 199-205.

Conference presentation (2011-2013)

1. Nuengruethai Ekthammathat, Titipun Thongtem, Anukorn Phuruangrat and Somchai Thongtem, "Luminescence of uniform $LaPO_4$ nanorods synthesized by a facile microwave method", The 28th Annual Conference of the Microscopy Society of Thailand (MST-28), 5-7 January 2011, Mea Fah Luang University, Chiang Rai, Thailand.
   (Proceeding of the 28th MST Annual Conference)
2. Nuengruethai Ekthammathat, Titipun Thongtem, Anukorn Phuruangrat and Somchai Thongtem, "Luminescence of uniform $LaPO_4$ nanorods synthesized by a facile microwave method", The International Congress for Innovation in Chemistry, 4-7 May 2011, Pattaya, Chonburi, Thailand.
   (PERCH-CIC Congress VII)
3. Nuengruethai Ekthammathat, Titipun Thongtem, Anukorn Phuruangrat and Somchai Thongtem, "Microwave-assisted synthesis of $CePO_4$ nanorods phosphor with violet emission", The 12th International Symposium on Eco-materials Processing and Design (ISEPD-12), 8-11 January 2011, Chiang Mai University, Chiang Mai, Thailand.
   (Excellence Award of Poster Presentation)
4. Nuengruethai Ekthammathat, Titipun Thongtem, Anukorn Phuruangrat and Somchai Thongtem, "Growth of hexagonal prism ZnO nanorods on Zn substrates by hydrothermal method and their photoluminescence", The 8th Asian Meeting on Electroceramics (AMEC-8), 1-5 July 2012, Penang, Malaysia
   (Oral Presentation)

Academic awards

1. Excellence Award of Poster Presentation, Microwave-assisted Synthesis of $CePO_4$ Nanorods Phosphor with Violet Emission, ISEPD 2011.